https://ntrs.nasa.gov/search.jsp?R=19790011969 2020-03-21T23:06:58+00:00Z

CR-152238

FEASIBILITY STUDY OF

TRANSIT PHOTON CORRELATION ANEMOMETER

FOR AMES RESEARCH CENTER UNITARY WIND TUNNEL PLAN

FINAL REPORT

by

W. T. Mayo, Jr.
A. E. Smart

7 February 1979

SDL No. 79-6397

Prepared for:

NATIONAL AERONAUTICS AND SPACE ADMINISTRATION
Ames Research Center
Moffett Field, California 94035

Attention: Dr. Dennis Johnson

Under Contract No.:
NAS2-10072

ORIGINAL CONTAINS
COLOR ILLUSTRATIONS

SPECTRON
DEVELOPMENT
LABORATORIES
INC.

APR 1979
RECEIVED
NASA STI FACILITY

(NASA-CR-152238) FEASIBILITY STUDY OF TRANSIT PHOTON CORRELATION ANEMOMETER FOR AMES RESEARCH CENTER UNITARY WIND TUNNEL PLAN Final Report (Spectron Development Labs., Inc.) 86 p HC A05/MF A01 CSCL 14B G3/09

N79-20140

Unclas
16699

3303 Harbor Boulevard, Suite G-3
Costa Mesa, California 92626 (714) 549-8477

TABLE OF CONTENTS

LIST OF FIGURES

LIST OF FIGURES

LIST OF TABLES

1.0 INTRODUCTION

A laser transit anemometer (LTA) measures a two-dimensional vector velocity by measuring the transit time of scattering particles between two focused and parallel laser beams. Spectron Development Laboratories, Inc. (SDL) has been active in the research and development of LTA systems. The objectives of this research contract were: (1) the determination of the concentration levels and light scattering efficiencies of naturally occurring, submicron particles in the NASA/Ames Unitary Wind Tunnel Plan and (2) the evaluation based on these measured data of a laser transit anemometer with digital correlation processing for nonintrusive velocity measurement in this facility. The criteria for the evaluation were to have been the speed at which point velocity measurements could be realized with this technique (as determined from computer simulations) for given accuracy requirements.

Prior to the NASA contract award, SDL constructed a developmental prototype LTA system under contract to the Arnold Engineering Development Center. The SDL LTA system was subsequently used to make data rate measurements in the NASA Ames 6-foot x 6-foot transonic wind tunnel during the middle of October, 1978. Specifically, backscatter velocity measurements were obtained without seeding with mean velocity repeatability of 0.15 percent in four successive runs of 5 seconds each while 'on condition' at Mach 0.9, Reynolds Number 3×10^6/foot. Additional measurements were made up to Mach 1.6.

In this report we briefly describe the SDL LTA apparatus, the measurements at NASA Ames, the data collected, and its interpretation with SDL computer software and computations, theoretical scaling equations for data rate, and the system design parameters for a larger-scale system with a range of 2 to 3 meters.

2.0 HISTORY AND DESCRIPTION OF SDL LTA SYSTEM

2.1 Historical Introduction

Initial laser velocimeter (LV) experiments in this country were made with heterodyne (reference beam) optical systems using frequency tracking electronics. The dual-beam (fringe) optical systems and classical-signal burst-counter electronics have proven to be more applicable to high-speed air flows and have been used with success.

During the last several years, LV systems have been extensively developed and applied to practical supersonic and transonic flow measurements. These measurements have been made in the inviscid region and within turbulent boundary layers with separation[1,2].

Particle lag problems are sometimes encountered in aerodynamic LV measurements[3,4]. Unseeded (or even filtered) air contains a very large number of submicron particles which are sufficiently small to follow high accelerations in the flow*, but obtaining adequate backscatter single-particle signal-to-noise ratios for classical burst-counter measurements is difficult even with the higher powered argon lasers.

Schodl and others elsewhere have been developing the rather old idea of a two-spot system in which the probe volume consists of a

---

* W. T. Mayo has reported measurements of large numbers of particles in the 0.2 - 0.8 micrometer diameter range in the laboratory air at the AEDC[5,6].

pair of parallel highly focused laser beams[7] and a matched receiver instead of the now common dual-beam fringes. A. E. Smart reported measurements with a different type of two-spot system at Cambridge in 1977[12]. The advantages include much less total probe volume and much higher focused laser beam intensity; and both of these qualities enhances sensitivity to small particles while decreasing the probability of intercepting the more sparsely distributed large particles. In addition, the higher resolution spatial filtering provides much better background light (flare) rejection when measurements near bodies are desired.

Photon correlation has been known to be ideally more sensitive than classical detection for several years. The techniques and theory for fringe LV systems are reviewed in References 6-10. Unfortunately, the available correlator electronic speed has not really been adequate* to be compatible with transonic speeds and the simultaneous demands for small probe volumes. An LTA system has a great advantage here. It achieves lower electronic bandwidth requirements while increasing the small-particle SNR and isolation. The reduced bandwidth makes the use of a 50 nsec Malvern correlator feasible for supersonic velocities. Thus, the *combination* of two-spot techniques and digital correlation offers exceptional improvements in small-particle sensitivity and is practical at supersonic velocities.

---

* John Abbiss has made supersonic measurements at the R.A.E. in England but with large fringe spacing appropriate for the 50 nsec resolution of the Malvern Instruments correlator[9].

A. E. Smart, formerly of Rolls-Royce, Derby, England, has taken advantage of these compatible techniques (two-spot and digital correlation) and extended them in some rather clever ways[11-12]. He designed, constructed, and used a system employing a small helium neon laser to make backscatter measurements in both subsonic flows and supersonic flows. The details of the Rolls-Royce instrument, which is capable of mapping out the two-dimensional u-v velocity probability function for statistically stationary flows, are proprietary to Rolls-Royce and have not been released. However, Dr. Smart has joined SDL and assisted W. T. Mayo in the development of a new argon-laser transit anemometer system under Contract F40600-78-C-0002 for the U.S. Air Force Arnold Engineering Development Center.

In previous NASA, AEDC, and ARPA sponsored research, W. T. Mayo, Jr. has developed extensive laser velocimeter computer simulation and design software[15-17], photon correlation interpretation software[18], and specialized photon correlation hardware[19-21].

During the period March 1978 through August 1978, SDL has developed a completely new laser transit anemometer system. The SDL LTA system utilizes a unique f/4 mirror-dove rotator/derotator prism for aberration-free spot pair rotation. The system includes newly developed pulse discriminators which operate to estimate the pulse center independently of the signal amplitude from classical signals down to photon resolved signals. New fiber optic techniques are utilized to improve receiver efficiency and probe volume depth restriction. The system rotation optics, the discriminators, and

the correlator are all under microcomputer control; and the microcomputer displays and provides first-order data interpretation to the user in semi-real time while storing all raw data for later detailed analysis by a larger computer. Figures 1, 2, and 3 illustrate the new SDL LTA optical head. The details of the system design are being reported separately in the AEDC Contract F40600-78-C-0002 final report (in preparation), but a system overview is presented in the following section which will be useful in understanding what follows.

2.2 Description of System Used for NASA Ames Experiment

The SDL LTA system, partly shown in Figures 1-3, was transported to NASA Ames on October 11, 1978, and set up as shown schematically in Figure 4. A 50 ns Malvern correlator (48 store) was used for the high-speed delay processing of the SDL pulse discriminator output signals. The correlator was used in both the 'photon' and the 'pulse' correlation modes and all the indistinguishable states in between as discussed further below. The laser was a Lexel Model 75-2 operating at about 135×10^{-3} W at 514.5 nm with 100×10^{-3} W in the transmitted beams.

The parameters of the SDL optical head were as follows. The spot separation was measured with a calibrated microscope objective as 376×10^{-6} m with $1/e^2$ spot diameters estimated at 1/25 of the spot separation, i.e., 15×10^{-6} m. The 'throw' or range from the front face of the optical head to the probe volume center was 473×10^{-3} m. The transmitter/receiver lens pair were 40×10^{-3} m in radius. The outer

ORIGINAL PAGE IS
OF POOR QUALITY

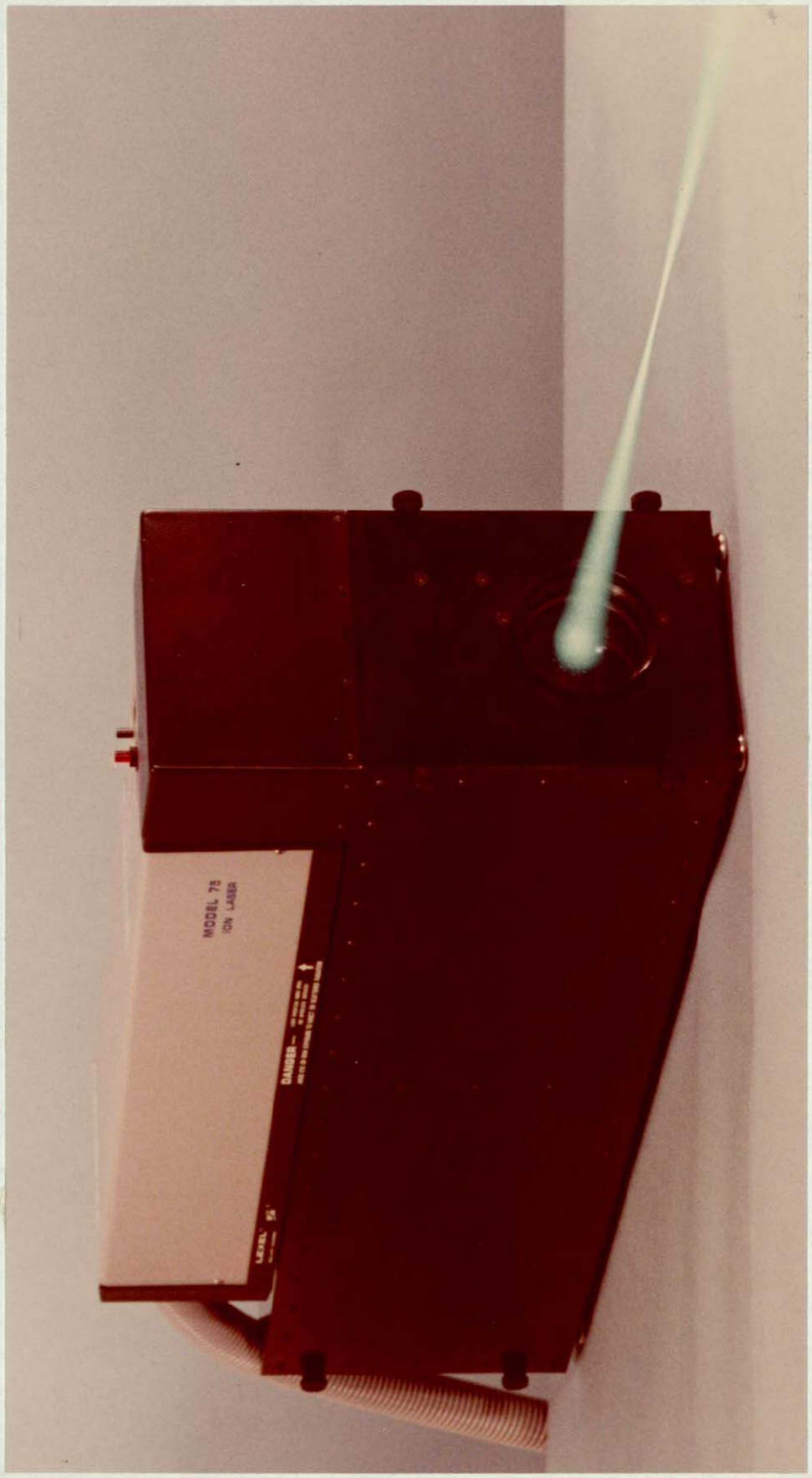

Figure 1. Overview SDL Laser Transit Anemometer (LTA) Optical Head.

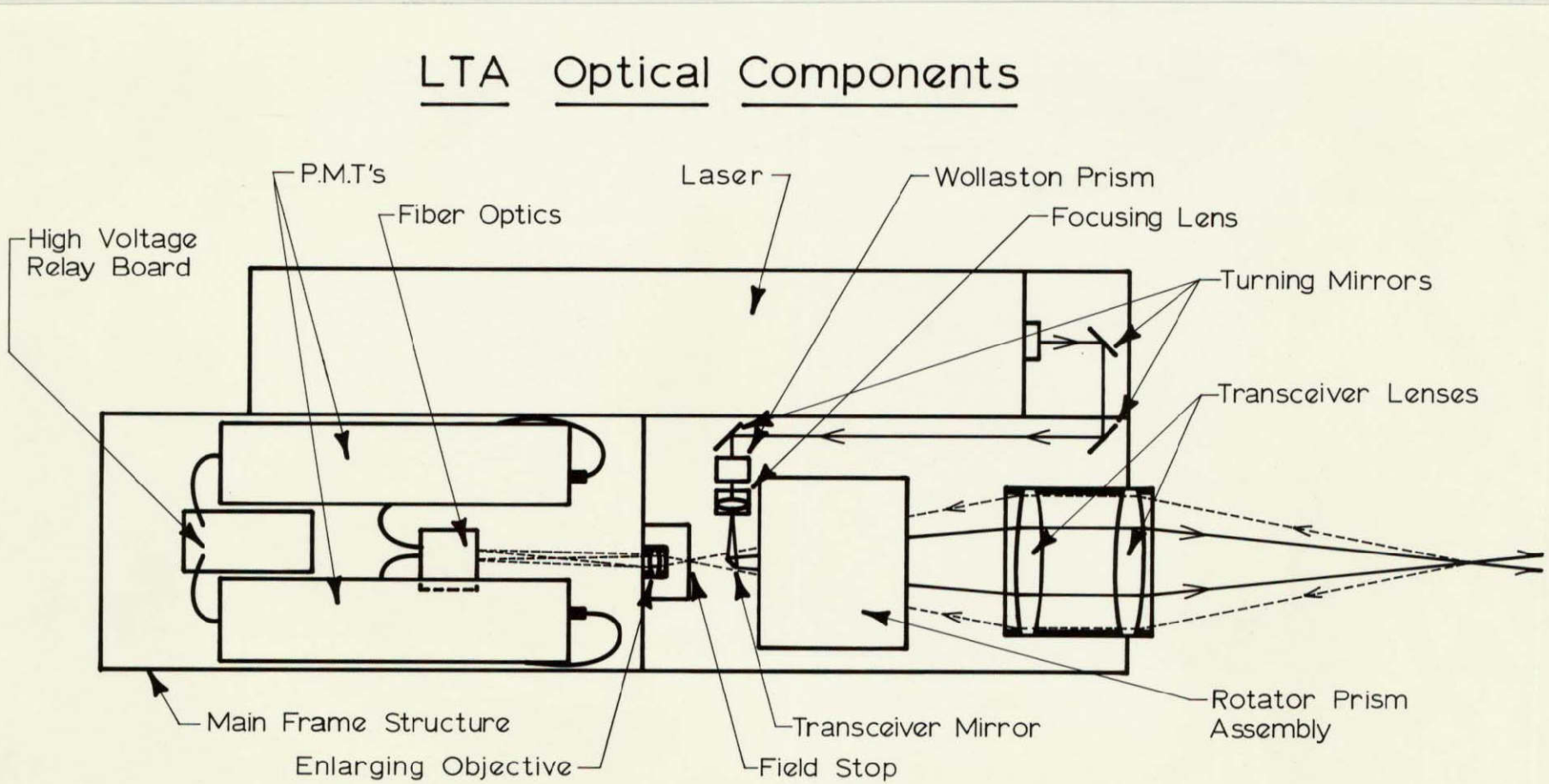

Figure 2. Schematic Diagram of Optical Components in SDL Optical Head.

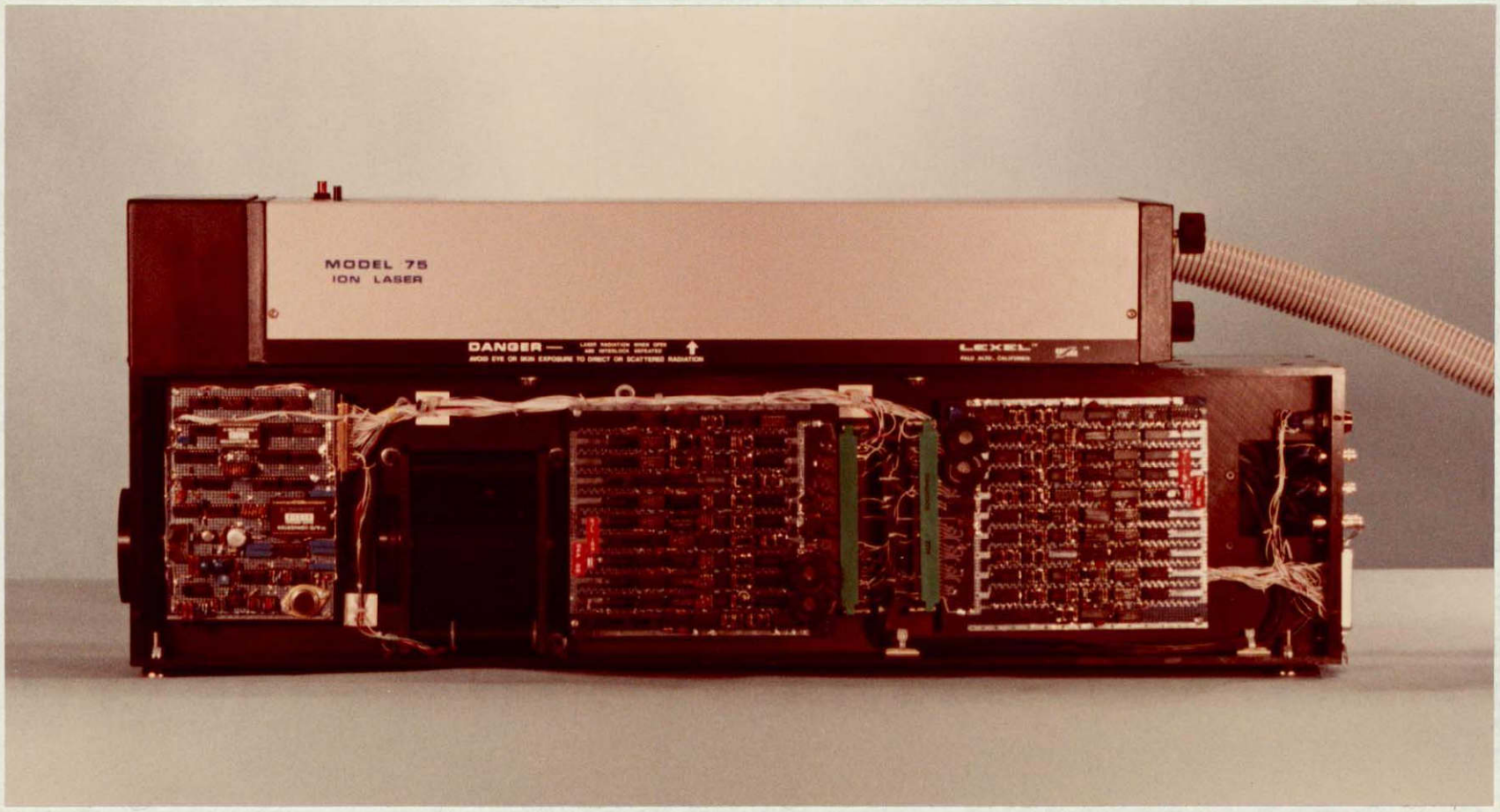

Figure 3. SDL LTA Electronic Components.

ORIGINAL PAGE IS
OF POOR QUALITY

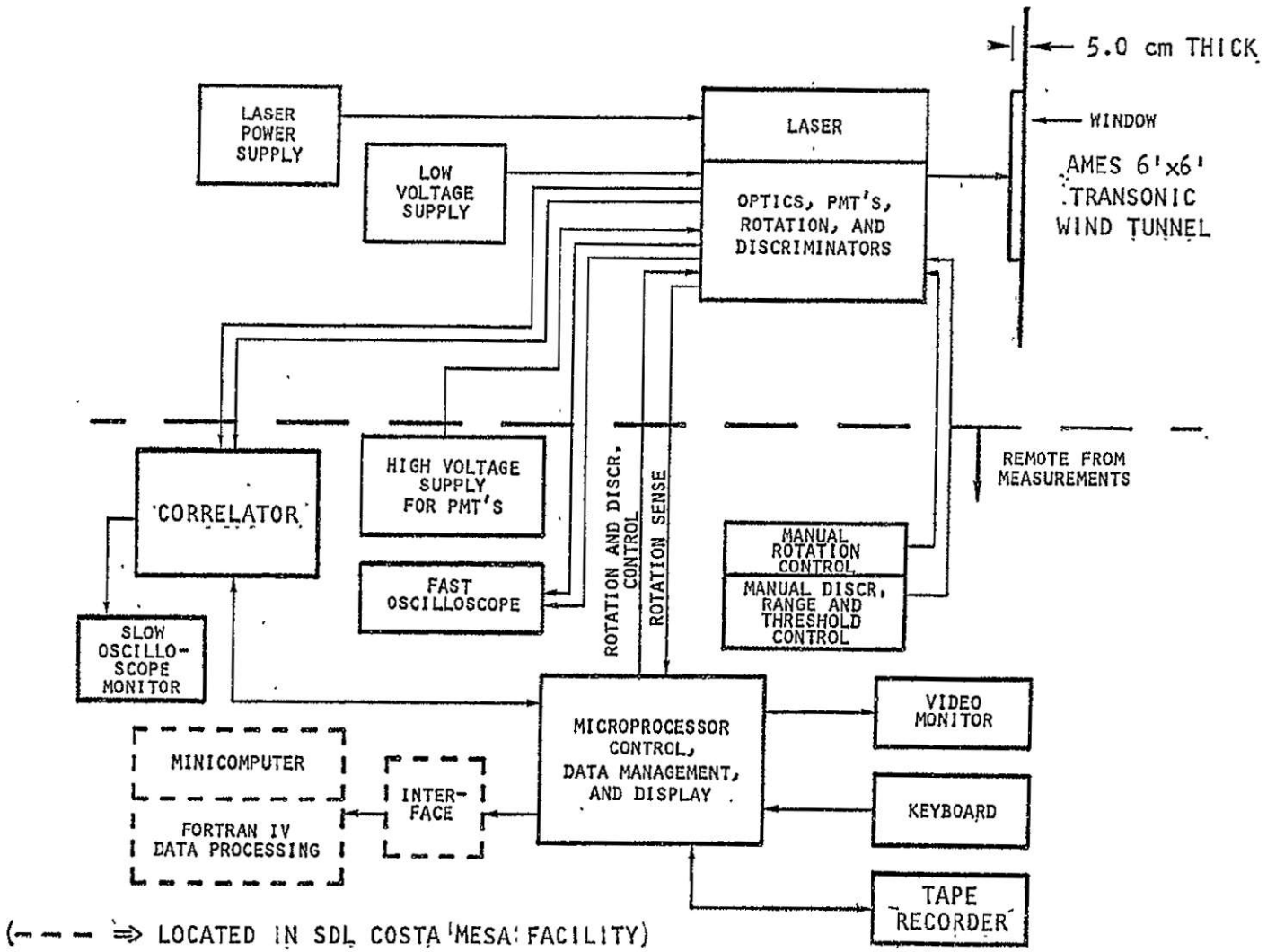

Figure 4. Block Diagram of SDL LTA System for Ames Transonic Measurements.

annular portion of the lens from radius 20×10^{-3} to 40×10^{-3} m radius was used for the receiver, while the inner area from 0 to 20×10^{-3} m radius was used for the transitted beams. The transmitter/receiver rotator prism assembly has digital-to-analog DC drive with DC feedback sensing, and a separate linear potentiometer and analog-to-digital readout. The precision of this angular control system is 0.1 degree.

The co-annular backscattered radiation is imaged around a small transmitter beam turning mirror to two pinhole aperture stops which transmit the desired signal radiation and some diffuse background radiation to a microscope objective which magnifies the images of the transmitted beams illuminating scatterers onto the ends of two fiber optics assemblies. The purpose of the fiber optics is to separate the light from the two spots to two separate photomultiplier tube detectors, one for each spot*. The use of two detectors provides completely unambiguous direction sensing capability and also avoids a zero delay correlation which would interfere with data processing in high turbulence conditions. Perhaps the most subtle advantage of two detectors is that the effective background light is one-half for each detector over what would occur is both spots were imaged on the same tube. Thus, the undesired background for the cross correlation of two detector outputs is one-fourth that of the autocorrelation of one detector output with both signals.

---

* For these experiments EMI 9816 and an EMI D305 tubes were used. Both tubes are 2" diameter, 14 stage, S-20 tubes of high quality.

The pulse detection discriminators include several overlapping ranges. Range 1 is optimized for pulses with duration 25-100 nsec; Range 2 for 50-200 nsec; Range 3 for 100-400 nsec, and so forth for seven ranges. Each range includes separate optimum detection filters, which are flat in response across the range so as not to bias the detection probabilities towards higher or lower velocities, and pulse center detection filters which determine the center of the pulse independently of signal amplitude.

For signal pulses which contain only one, two, or a small number of single photoelectron pulses, the pulse center detection filter measures a crude weighted average pulse center estimation. This means that pulse center jitter errors can occur up to the transit time duration as the number of detected photons goes down to one. This implies a distinct precision advantage of working with three or more photoelectron pulses per scatterer transit both to avoid processing so many single photoelectron signals arising purely from background light and to reduce the pulse-center estimation error. In order to use semi-classical and classical pulse techniques, one raises the detection threshold so that single photoelectron pulses are detected less often. However, due to the statistical distribution of single photoelectron pulse heights from the PMT electron multiplier, the transition from single to multiple photoelectron events is not distinct, as the data discussed later shows.

The discriminator detection range was both manually and microcomputer selectable from the remote location where the operator

station was located. The discriminator level and the PMT high-voltage were both manually remote controllable. The PMT's were protected from maximum anode current overload by high-voltage relays following an anode DC current monitor. These relays were remotely resetable (not shown in figure). The prism rotator also has remote manual control. Thus, using the correlator on manual with manual rotator and discriminator control, setup and checkout operations can be performed independently of the microcomputer. When the selector switches are set to microcomputer control, the control of the correlator start, data acquisition, and rotator control become automatic.

3.0 MEASUREMENTS AT NASA AMES

3.1 Pre-Tunnel Procedures

The system illustrated in Figures 1-4 was set up by W. T. Mayo and A. E. Smart with the optical head located on a table pointing into a two-inch thick schlieren quality window upstream of the primary test section of the 6' x 6' transonic wind tunnel. It was determined experimentally that less background counts from single-photoelectron signals were obtained ($\approx$ 800,000 per channel) when the optical axis was tilted slightly to avoid the direct window reflection back into the transceiver lens*; it was noted, however, that a perpendicular arrangement allowed operation with approximately 4×10^6 background counts per channel. These figures were measured prior to a change in the optics which preceded the measurements of October 17, and are thus only qualitatively useful. All of the final signal data was acquired on Range 2 (smaller effective gain by 2x) with the PMT voltages reduced to 1900 v and 1960 v for the two tubes, with thresholds from 50 mv to 400 mv. The resulting input pulse count rates were less than $200{,}000/s^{-1}$ in most cases due to the higher relative detection threshold.

One of the difficulties of the experiment was that the tunnel was inoperative for most of the first three days after the equipment was set up. A brief run just after setup indicated that data was being

---

* These were the final rates on October 17 and are large due to lens aberrations. Lower values are expected in the future.

obtained at transonic speeds, but the sensitivity was marginal. This fact and the down time provided incentive for a small modification of the system optics wherein the microscope objective which images the spots onto the fiber optics was reduced in power. Earlier laboratory measurements had indicated that the transceiver lenses were nearly diffraction limited over the transmitter central position but that the effective blur circle of the receiver annulus was ten times larger in diameter. Since the design had assumed that the return primary image was the matched size, the actual scatter images on the ends of the fiber optics were too large, even though some reduction had already been accomplished. The additional change of imaging objective reduced the image to only about three times the diameter of the fiber. This increased the sensitivity noticeably.

To further quantify the degree of difficulty arising from the loss between the input and output of the fibers, an experiment was conducted in which a small NASA-owned low-gain photomultiplier tube was used to measure separately the light imaged from a finely diffused metal surface in the probe volume center before entering and after leaving the fiber optics assemblies. It was difficult to perform this measurement precisely due to the necessity of using a dentist mirror to get the light that would have imaged into the fibers to image into the pinhole of the test PMT. Also, there was indication that the tube was saturating slightly, even at the lowest available laser power setting. In spite of these considerations, the results showed that only about 1/10th of the available light was reaching the PMT's.

This is consistent with our visual observation that the scatter image appeared nearly three times wider than the end of the fibers. We have performed laboratory experiments which indicate that the short focal length internal lens has most of the aberrations. This will be corrected in future systems.

3.2 Tunnel Meausrements: Group 1, October 16, 1978

When the tunnel was again operated, it was swing shift on October 16, 1978. The tunnel was operated at a variety of Mach numbers from 0.6 to 1.6 at both Reynolds Number 1.5×10^6 and 3.0×10^6/ft. The system appeared to perform very well. A variety of system parameters were adjusted and the following general selections for each run were made:

Discriminator Range:	2
Sample Increment:	50 ns
No. of Samples:	10^8
Total Time	5 s
HV PMT A:	1900 v
HV PMT B:	1980 v
Discriminator Thresholds:	50, 70, 100, 140, 200, 280, 400 mv.

It was observed that easily discernible signal correlation peaks could be obtained with 0.5 s and even 50 ms runs during subsonic runs with Reynolds Number = 3×10^6/ft. During the initial run, the Mach number was up to Mach 1.6, Reynolds Number = 1.5×10^6/ft, and large amounts of condensation occurred. Visibility into the lighted test section

downstream was poor. The PMT protect relay tripped, and the high voltage was reduced to 1800 v and then 1600 v. Good signal correlations were obtained at 1600 v with threshold at 280 mv.

During the Group 1 experiments, the effects of threshold changes were noted and also the effects of angle rotation. Since the probe volume was located approximately 20 cm into the free-stream flow, the turbulence level was very low and the angular increments were quite small. The data from these runs was presumably recorded, with a few auxiliary hand written notes concerning run numbers and threshold settings. Unfortunately, examination of the contents of the tape recordings the next morning (October 17, 1978) revealed that a minor software error had been made in final changes just prior to transporting the equipment which not only was not detected in the setup procedures but also caused all the data from the Group 1 experiments to not be saved. Thus, during the day of October 17, 1978, the software was modified in preparation for the experiments during swing shift on Tuesday, October 17, 1978.

3.3 Tunnel Measurements: Group 2, October 17, 1978

The scheduled tunnel runs for October 17 were to be a sequence of many conditions with only about one minute for each condition. (It takes 10-15 minutes to get from one condition to another, but they were not going to hold on each condition very long.) However, it was agreed that the condition of Mach 0.9 would be held for 10 minutes at each of the Reynolds numbers 1.5 and 3.0×10^6/ft so that SDL

could take repeated measurements with the tunnel 'on condition.' Data sheets were Xeroxed with the general parameters previously determined already written in so that the investigators could concentrate on writing down the measured count rates on Channels A and B (using the correlator manually) and tape record the correlograms and other data for many different threshold settings at the same condition. Some of the data was taken while the tunnel was changing from one condition to another, but several sequences were obtained 'on condition' at Mach 0.9 at both Reynolds numbers. Generally, the data rates were higher for the higher Reynolds number condition.

3.4 Data Presentation: Group 2

Upon return to the SDL Costa Mesa facility after the data collection on the evening of October 17, 1978, the data tapes were transferred to the SDL HP 21MXE System 1000 computer for plotting and data analysis. The raw data is reproduced in the appendix which contains plots of the correlograms (simple straight line connections between points, not curve fits).

Spectron has software which uses nonlinear regression techniques to fit data to analytic functions with parameters. Figures 5 through 11 illustrate the results of first subtracting the mean baseline (points outside the peak) and then fitting a 3-parameter Gaussian curve (amplitude, mean, and rms width) to the five values near the peak. The results indicate dramatically that the determination of the mean delay can be much more precise than the 50 ns time delay increment.

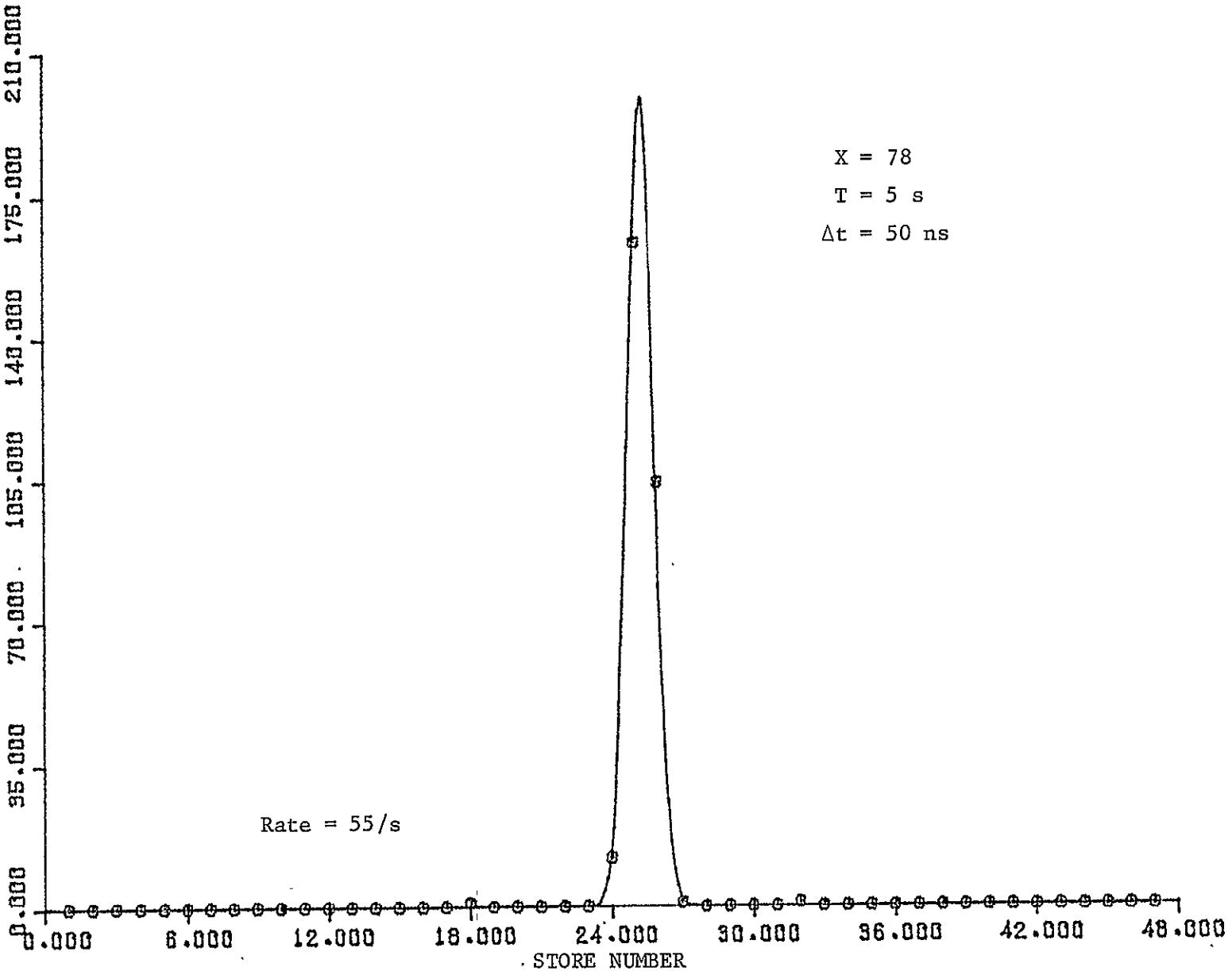

Figure 5. Curve Fit of Correlogram at M = 0.9, Threshold = 400 mv.

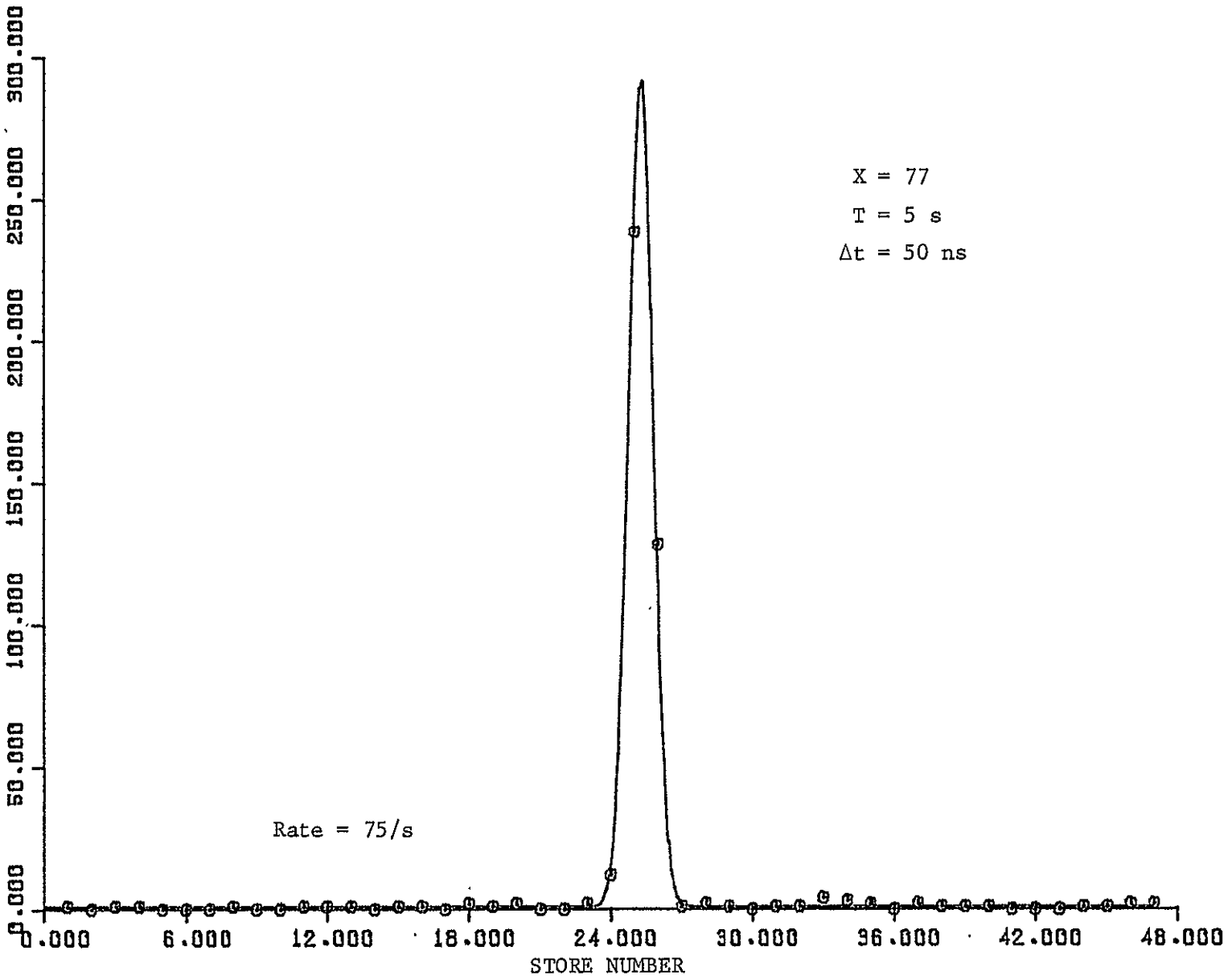

Figure 6. Curve Fit of Correlogram at M = 0.9, Threshold = 280 mv.

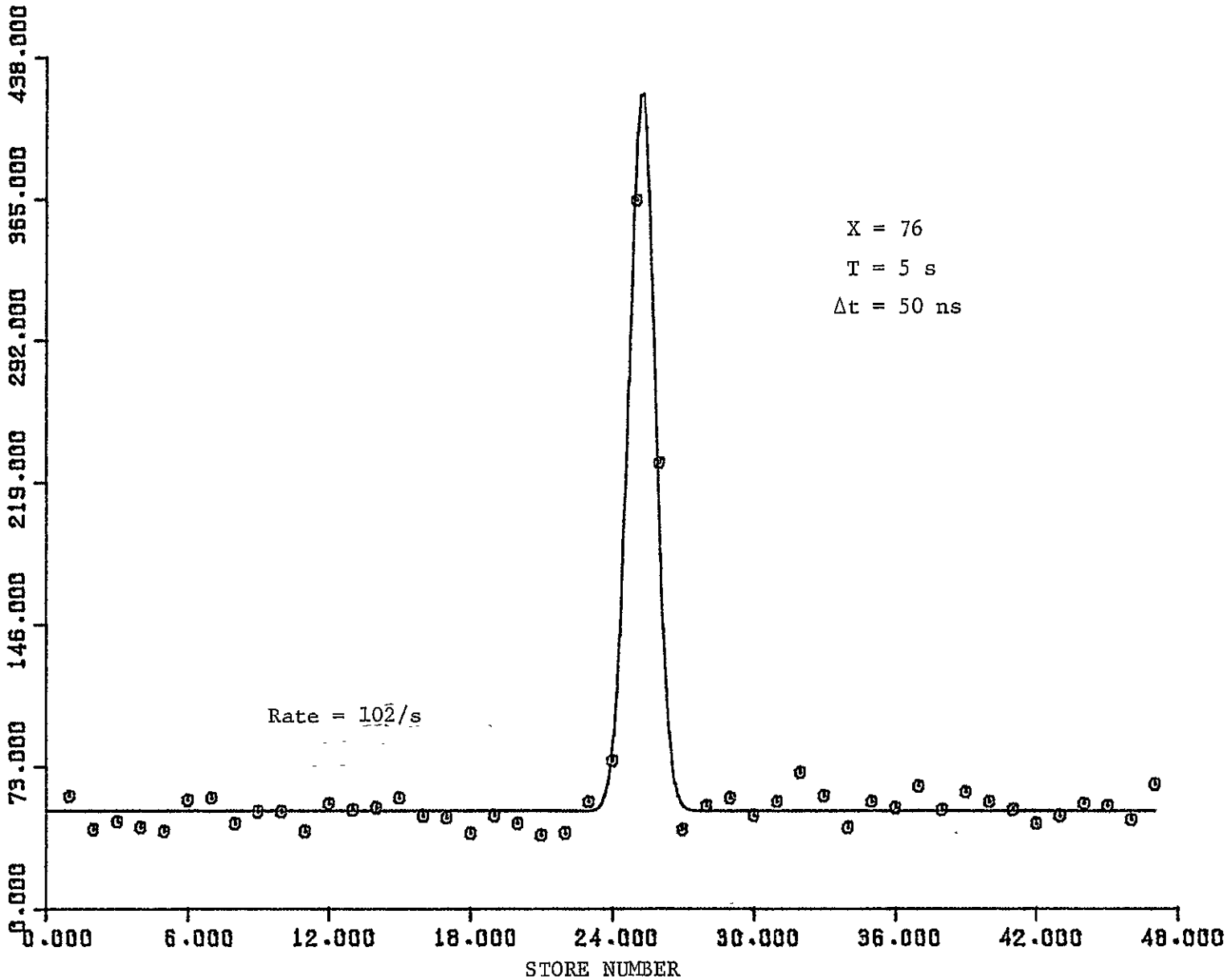

Figure 7. Curve Fit of Correlogram at M = 0.9, Threshold = 200 mv.

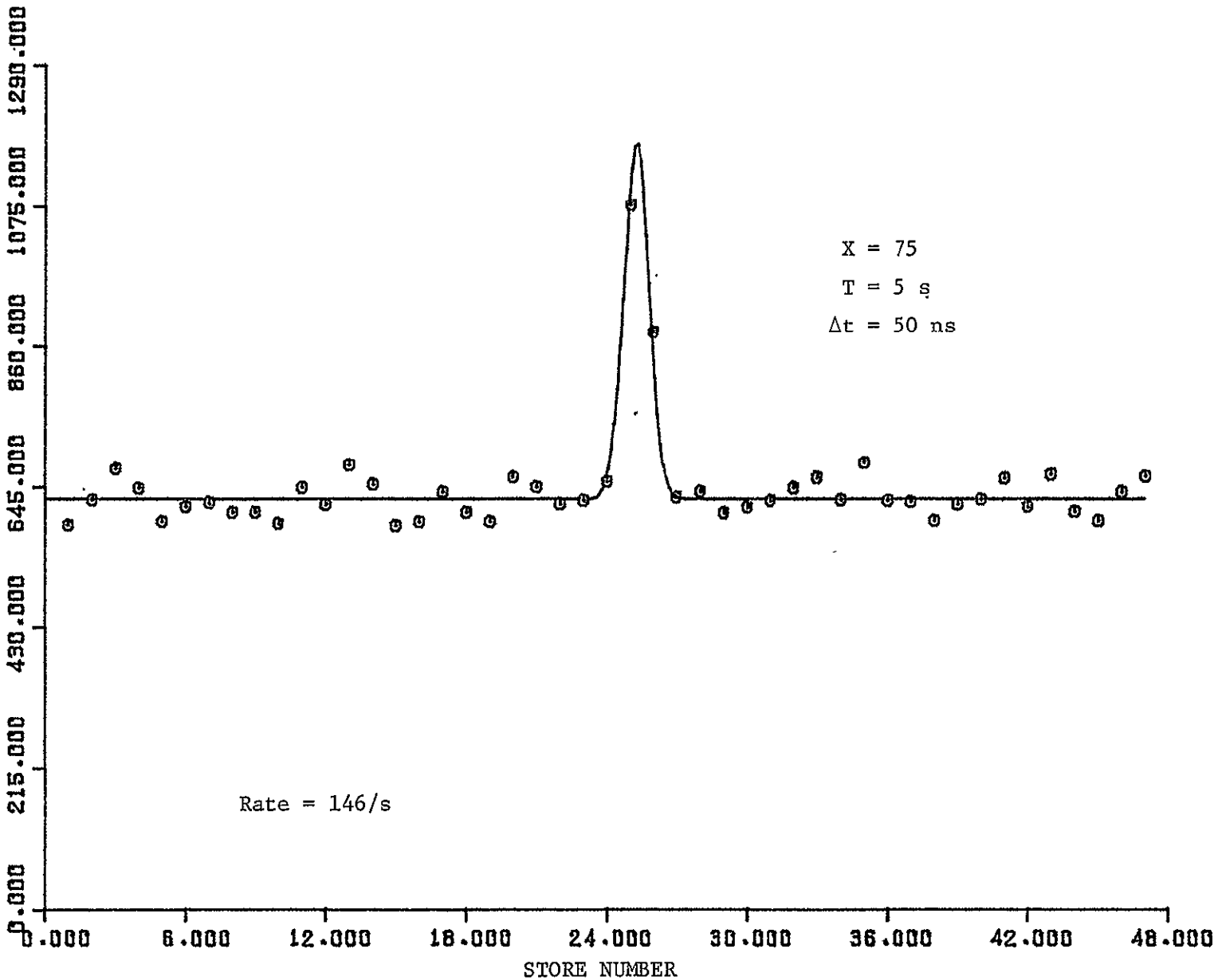

Figure 8. Curve Fit of Correlogram at M = 0.9, Threshold = 140 mv.

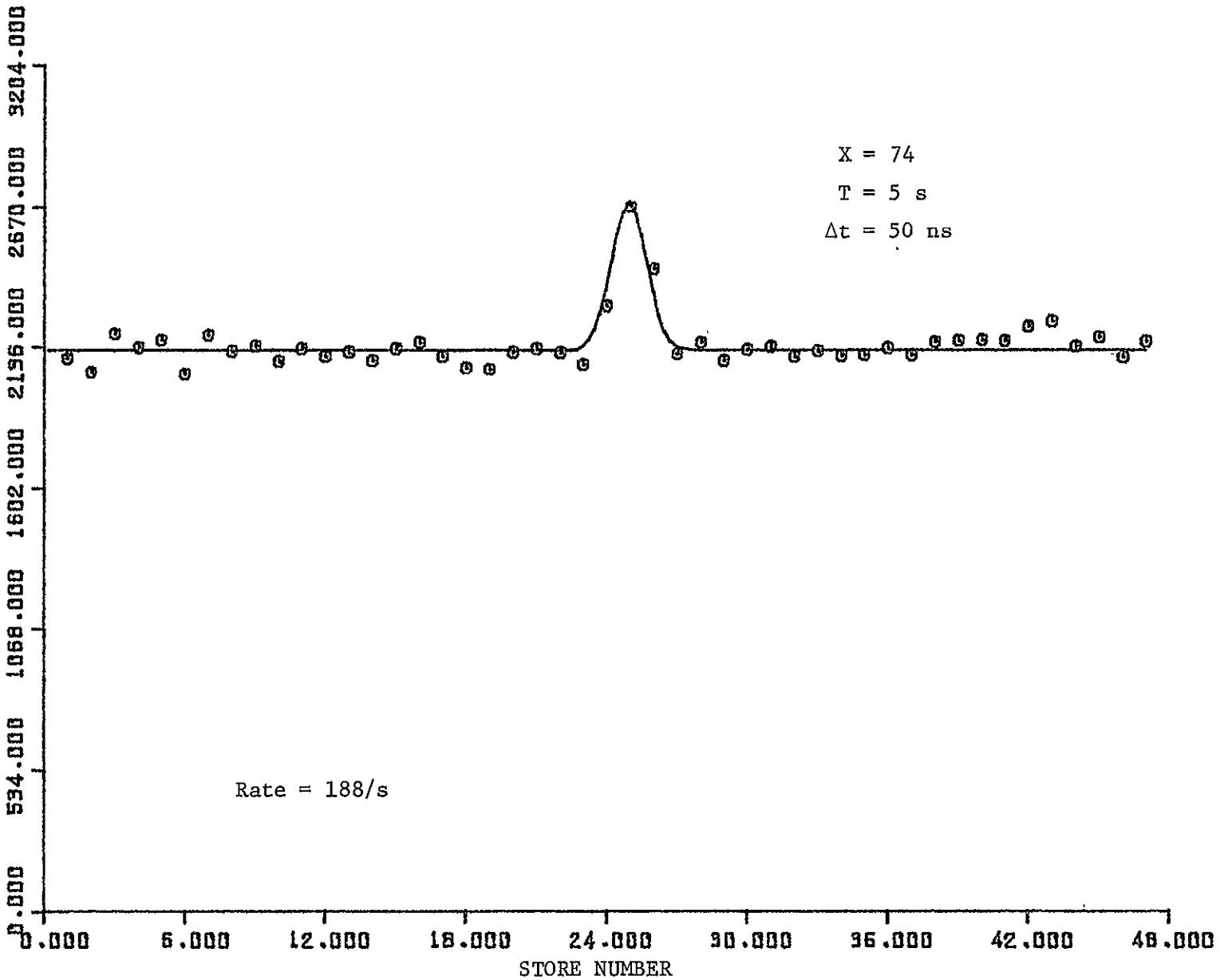

Figure 9. Curve Fit of Correlogram at M = 0.9, Threshold = 100 mv.

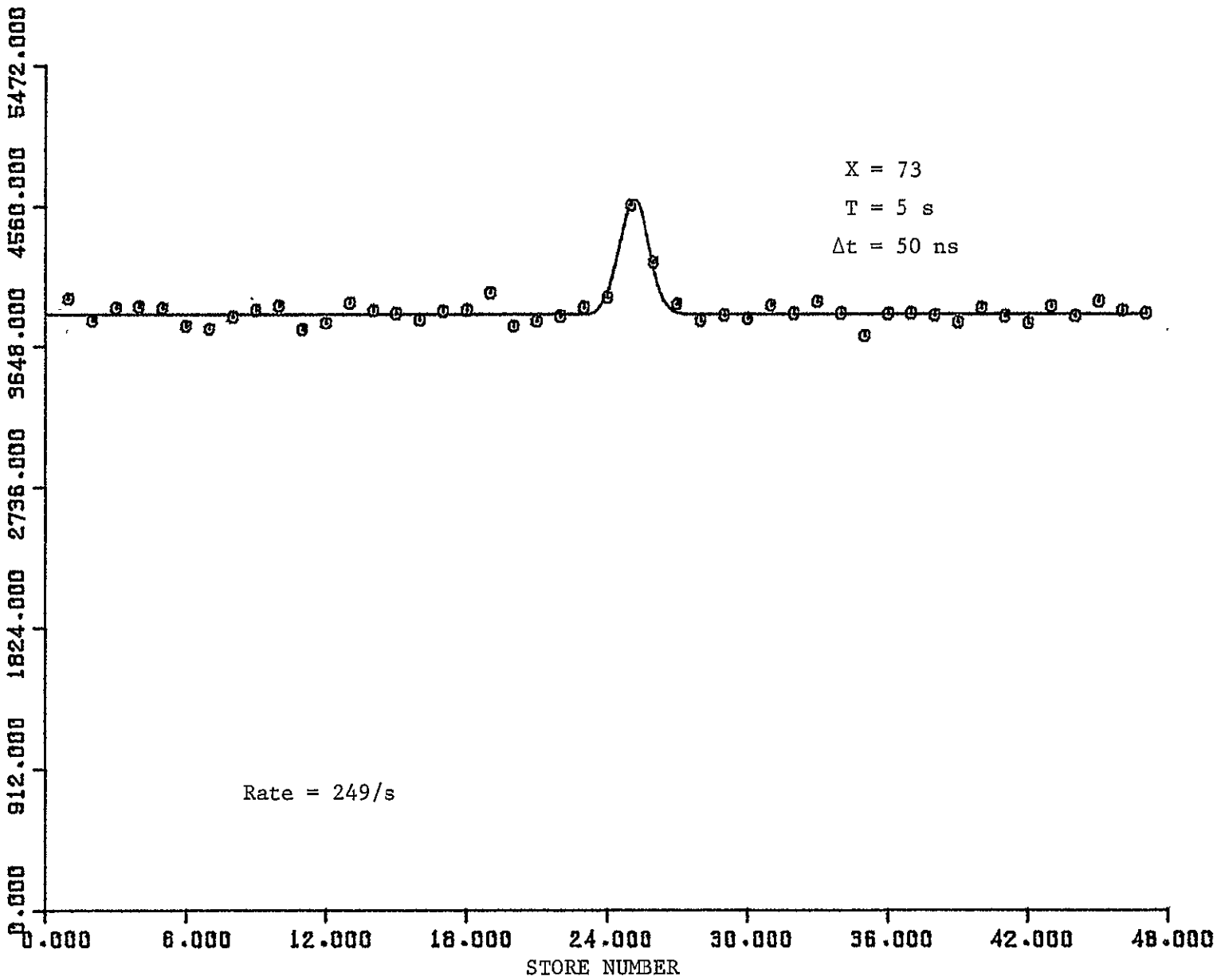

Figure 10. Curve Fit of Correlogram at M = 0.9, Threshold = 70 mv.

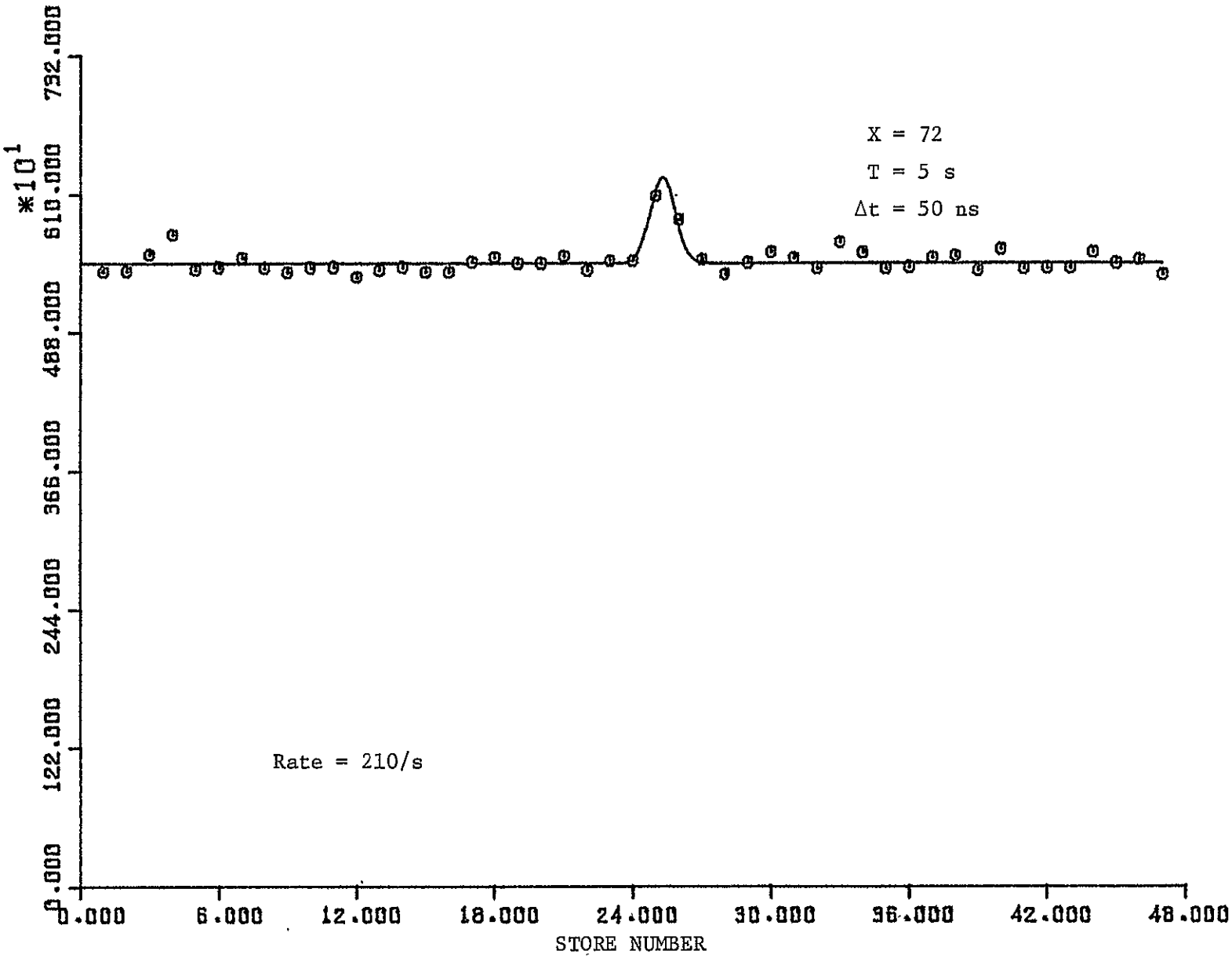

Figure 11. Curve Fit of Correlogram at M = 0.9, Threshold = 50 mv.

The apparent rms turbulence intensity was typically 2 to 3 percent in these runs. These figures are high because they *are* affected by the 50 ns delay increment of the correlator. The results of applying the curve fit software to all of the data runs is summarized in Table 1.

The fluctuations in apparent turbulence intensity represent the effects of tunnel velocity drift over 5-second intervals, photon noise, discriminator jitter, etc. The basic width of 4 percent due to the 50 ns delay increment results in an apparent rms width of approximately 2 percent. Figure 12 indicates very small changes of apparent turbulence intensity over two sets of runs 'on condition' at Mach 0.9, Reynolds number 3×10^6/ft. It appears that the apparent turbulence intensities may be corrected by subtracting the correlator time resolution effect from the mean square deviation; however, such an analysis is beyond the scope of this report. The purchase of a faster correlator would be of assistance in making very low turbulence measurements.

The 'background' presented in Table 1 is the mean value of the flat background level in the correlograms (5 seconds of data). The 'data rate' is the sum of the correlogram stores near the peak minus the background level, the quantity divided by 5 seconds. Thus, the sum of the correlogram values above the background in Figures 5-11 are obtained by multiplying the 'data rate' by 5 seconds for the appropriate run number.

Attention is called to the sequence of runs 75 through 78. These four successive runs show a repeatability of the mean flow

RUN X	THRESHOLD (VOLTS)	DATA RATE	BACKGROUND	MEAN VELOCITY	TURBULENCE INTENSITY
1	.5000E-01	44	5480	OVERFLOW	
2	.7000E-01	50	4030	OVERFLOW	
3	.1600E+00	116	2394	299.765	.0249
4	.1400E+00	50	805	300.227	.0490
5	.2000E+00	23	78	293.826	.0014
6	.2820E+00	24	1	297.103	.0200
7	.4000E+00	17	0	297.365	.0171
8	.4000E+00	21	0	352.891	.0202
9	.2820E+00	35	0	355.081	.0230
10	.2000E+00	53	7	351.450	.0227
11	.1400E+00	74	208	355.709	.0272
12	1.0000E-01	110	1142	356.329	.0323
13	.7000E-01	94	2744	OVERFLOW	
14	.5000E-01	96	4485	401.340	.0292
15	.2000E+00	48	45	356.107	.0235
16	.1400E+00	53	631	357.244	.0235
17	1.0000E-01	85	2028	385.349	.0251
18	.7000E-01	278	3787	OVERFLOW	
19	.2820E+00	30	0	393.338	.0258
20	.4000E+00	4	0	395.789	.0277
21	.4000E+00	6	0	384.095	.0185
22	.2820E+00	41	1	385.350	.0262
23	.2000E+00	336	155	408.364	.0295
24	.1400E+00	9273	16045	417.701	.0329
25	.2450E-02	100986	674147	427.475	.0207
26	.4000E+00		3	OVERFLOW	
27	.4000E+00	2801	1863	387.444	.0245
28	.2820E+00	86	0	316.622	.0216
29	.2000E+00	158	35	330.629	.0236
30	.1400E+00	289	568	332.697	.0257
31	1.0000E-01	390	2064	332.982	.0268
32.1	.4000E+00	73	0	331.754	.0226
32.2	.4000E+00	72	0	309.783	.0194
33	.2800E+00	106	0	302.349	.0204
34	.2000E+00	139	43	301.901	.0223
35	.1410E+00	175	603	OVERFLOW	
36	1.0000E-01	230	2099	300.846	.0256
37	.7000E-01	189	3851	299.525	.0244
38	.5000E-01	185	5372	298.617	.0251
39	.4000E+00	22	0	294.382	.0185
41	.4000E+00	9	0	294.196	.0149
42	.2800E+00	9	0	297.400	.0268
43	.2000E+00	16	47	297.074	.0344
44	.1400E+00	6	618	OVERFLOW	
45	1.0000E-01	33	2071	OVERFLOW	
46	.4000E+00	5	0	295.110	.0144
47	.2820E+00	6	0	296.209	.0267
48	.2000E+00	7	40	OVERFLOW	
49	.1400E+00	30	570	197.706	.0156
50	.4000E+00	6	0	287.325	.0200

Table 1. Tabulation of Mean Velocity, Data Rate, and Apparent Turbulence Intensity Curve Fit.

RUN #	THRESHOLD (VOLTS)	DATA RATE	BACKGROUND	MEAN VELOCITY	TURBULENCE INTENSITY
51	.2820E+00	4	0	287.589	.0299
52	.2000E+00	7	40	OVERFLOW	
53	.1400E+00	22	598	274.557	.0007
54	.4000E+00	9	0	255.259	.0124
55	.2800E+00	10	0	253.085	.0180
58	.4000E+00	24	0	284.467	.0181
59	.2800E+00	24	0	290.207	.0217
60	.2000E+00	147	92	291.959	.0206
61	.1410E+00	116	629	293.594	.0273
62	1.0000E-01	149	2117	297.649	.0305
63	.7000E-01	184	3945	294.945	.0168
64	.5000E-01	220	5379	298.023	.0270
65	.4000E+00	51	0	294.884	.0177
66	.2820E+00	83	0	295.854	.0230
67	.2000E+00	91	49	295.372	.0209
68	.1410E+00	122	633	296.251	.0229
69	1.0000E-01	166	2131	296.139	.0222
70	.7000E-01	182	3912	OVERFLOW	
71	.5000E-01	302	5422	OVERFLOW	
72	.5000E-01	210	5489	296.342	.0213
73	.7000E-01	249	3860	298.220	.0249
74	1.0000E-01	188	2125	298.726	.0287
75	.1400E+00	146	626	296.840	.0214
76	.2000E+00	102	50	296.991	.0222
77	.2800E+00	75	0	296.861	.0205
78	.4000E+00	55	0	296.592	.0224
79	.4000E+00	119	0	199.999	.0160
80	.2820E+00	176	1	OVERFLOW	
81	.2000E+00	189	57	198.932	.0177
82	.1410E+00	243	673	196.378	.0195
83	1.0000E-01	324	2243	194.744	.0224
84	.7000E-01	339	4040	192.985	.0194
85	.5000E-01	357	5573	193.630	.0256
86	.5000E-01	261	5349	192.544	.0257
87	.7000E-01	323	3972	191.913	.0290
88	1.0000E-01	186	2240	193.005	.0185
89	.1400E+00	124	672	192.324	.0188
90	.2000E+00	93	53	192.353	.0179
91	.2820E+00	58	1	192.630	.0165
92	.4000E+00	43	0	192.869	.0146

* OVERFLOW indicates that the curve fit program did not converge. In come cases, the raw correlogram in the Appendix shows why in an obvious manner. A few cases merit further consideration of the choice of initial parameter selection for the software.

Table 1. Tabulation of Mean Velocity, Data Rate, and Apparent Turbulence Intensity Curve Fit (Concluded).

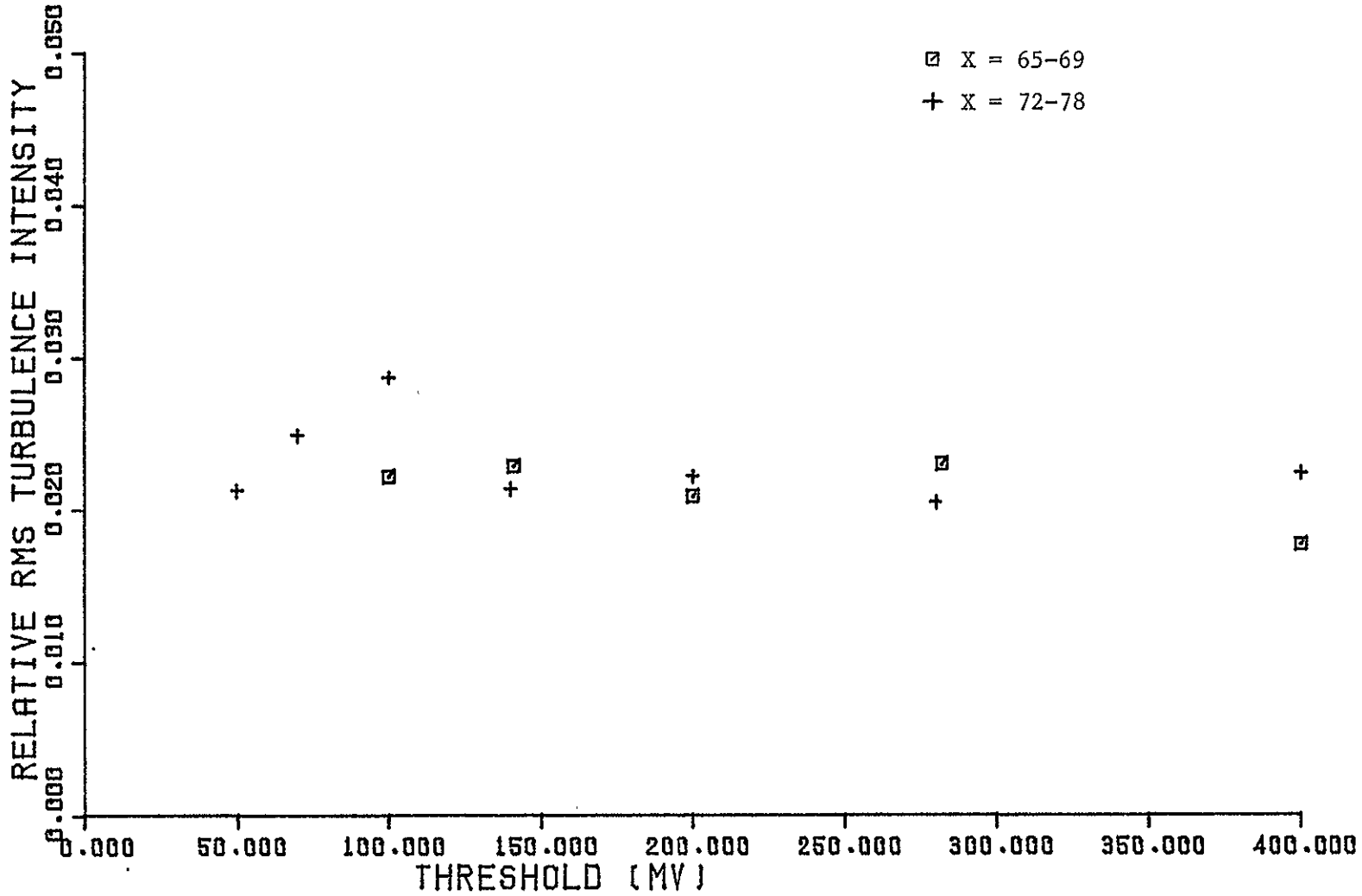

Figure 12. Apparent Turbulence Intensity on Condition at M = 0.9, Re. No. = 3×10^6/ft.

velocity measurement of better than 0.15 percent even though different discriminator thresholds were used. Other measurements while nominally 'on condition' show slightly less stability, but one cannot exclude that the tunnel velocity may have been drifting within small deviations also.

Before concluding this section, we should point out the comparison of our measured mean velocities with those obtained by the tunnel calibration computations. According to the tunnel computer, the actual Mach numbers, velocity in ft/sec, and Reynolds numbers during our runs X = 65 to 78 were:

Mach No.	V ($ft.s^{-1}$)	Rn/L
0.899	958.27	2.95
0.898	957.16	2.94
0.899	957.83	2.95

We must take into account that our measurements were made at a different location than the tunnel probes, and that we independently measured our spot separation to probably no better than 1 percent. Nevertheless, we have from the tunnel data (approximately the same time as runs 75-78 would have been made):

$$V\ (ms^{-1}) = 957.83 \times 0.3048\ m/ft = 291.9\ m/s$$

in contrast with our measured value of 296.8, i.e., a difference of 1.6 percent.

4.0 DATA ANALYSIS AND INTERPRETATION

Some of the original computational objectives of the proposed work have been surpassed by the experimental evidence. The primary case of this was our original intention to use single-beam scattering amplitude/rate data to predict by simulation some of the accuracy limitations of an LTA with correlation processing. The truth is that we could never have completely simulated all of the error sources and/or equipment limitations. The experimental mean-flow repeatability of 0.15 percent over four successive runs with 5 seconds of data each proves that excellent measurement precision is obtainable with a practical system. The facts that only an 80 mm diameter lens (whose aberrations cost an additional power loss of a factor of ten which should be recoverable), and a 135 mW laser was used indicates it should be possible to extend the system to a range of 2 meters (a factor of 4) by using 6 to 8 inch diameter high-precision optics.

Despite the feelings of certainty that the experiment has provided, we also need certain analytical and computational results to better understand the system performance limitations and to assist in scaling the design to larger ranges in the most useful manner. In this section we first examine the definition of the words 'data rate' and how this relates to different detection methods (photon vs. pulse correlation vs. pulse timing). This requires an examination of the nature of the pulse signals through simulation and computations of the system sensitivity to submicron particles. We finally consider, with simple

equations, the manner in which 'data rate' scales with lens diameter, focal range, and laser power. The statistical manner in which the detectability of signals reduces in the presence of wall flare is of great interest, but we must leave such studies until a later time.

4.1 Definition of Data Rate

Figure 13 is a reproduction of two oscilloscope photographs taken October 16. For these photographs, the signals from the Channel A and Channel B phototube monitors (10 ns pulse rise time) were summed electronically for display purposes. The maximum classical signals go to just over 2 volts where the preamps saturate. Careful observation of the original photographs shows a multitude of single photoelectron background pulses at the 50 to 150 mv level. Thus, as is obvious in the correlation data of Figures 5 through 11, when the pulse detection threshold exceeds the majority of the single photoelectron pulses, the background level of the correlation function goes to zero and only the classical signals which produce the correlation spike remain.

Using the above logic in reverse, one can imagine being convinced that when the correlation function appears to have little or no background, then the count rate of discriminator output pulses is equal to the data rate. As an example of this, we see in Figure 6 that the background is nearly zero. From the raw data for run X = 77, we found that the total counts into Channels A and B were

ORIGINAL PAGE IS
OF POOR QUALITY

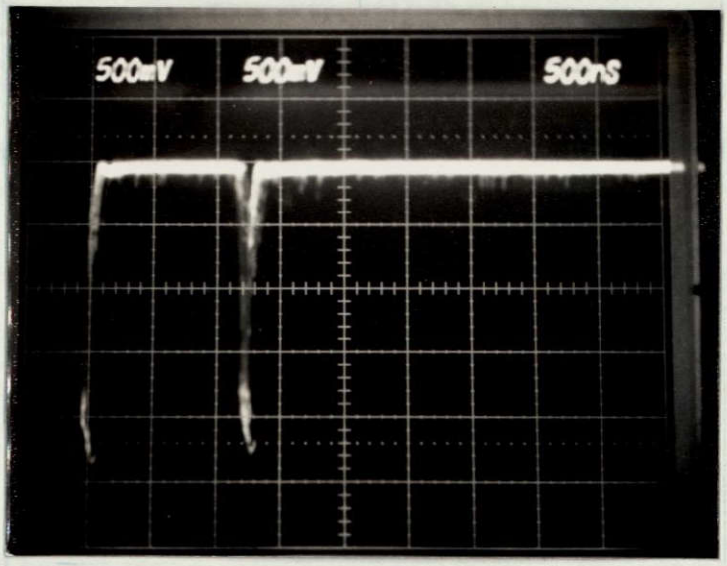

(a) Mach 0.9, Reynolds No. = $3x10^6$, 2 Second Exposure.

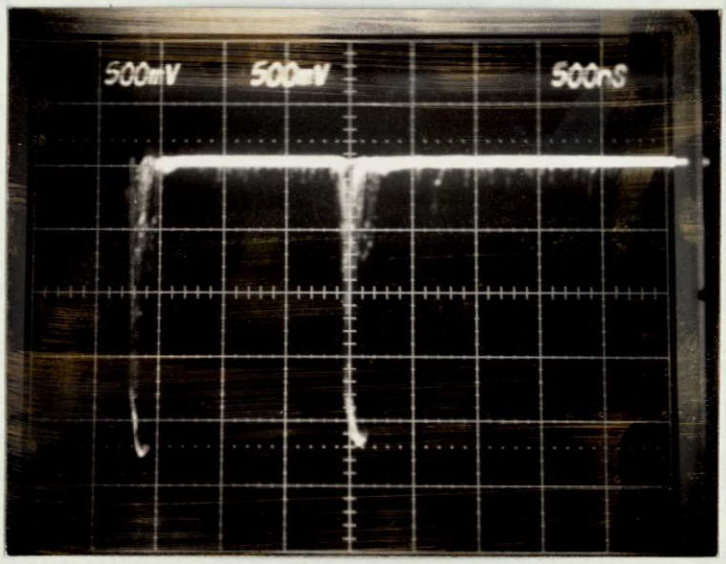

(b) Mach 0.7, Reynolds No. = $3x10^6$, 2 Second Exposure.

Figure 13. Oscilloscope Time Exposures of the Electronic Addition of Channels A and B Photomultiplier Tube Output Monitors, October 16, 1978.

6942 and 8584, respectively; so after dividing by 5 seconds, we deduce that the input pulse rates were 1388 s^{-1} and 1717 s^{-1}, respectively. However, we find from Table 1 that the data pair rate was only 75 s^{-1}. Could only 5 percent of the particles be passing through both spots? This is not reasonable since the tunnel turbulence is so low that nearly all of the scatterers which cross one spot should cross the other at nearly the same relative location; and this is evidenced by the gap in the baseline of the photograph in Figure 13(a) and many of the other photographs taken. (Unfortunately, none are available for run 77.) And to make the point a little more dramatically, we can consider run 76 (see Figure 7) where the input pulse rates were 15.24 Ks^{-1} and 12.76 Ks^{-1}, the correlation background is still far less than the correlation peak, and the data pair rate was only 102 s^{-1}.

The observed data indicate that a good correlogram peak to background ratio with 100 real data pairs s^{-1} in the presence of 15,000 s^{-1} Poisson random distributed pulses (both large amplitude single-photoelectron background pulses and single-photon signals from smaller particles which failed to produce a photoelectron for the other spot). It is clear from the above examples that data rate must be defined as the rate at which correlated pairs of pulses are detected by the pulse discriminator circuits, and that the *useful* data pair rate may be increased within limits by decreasing the threshold to include many uncorrelated pulses which would cause great inefficiency to any classical pulse pair timing circuits with any appreciable dead time.

4.2 Data Rate and Background Level Equations

For simplicity assume that all correlated pulse pairs occurred at exactly the same time delay. The rate of occurrence, on either channel, due to these 'signal' pulses is then λ_s. The height of the 'signal' part of the correlogram above the background level is thus $\lambda_s T$ where the sample duration T is given as

$$T = N\Delta t$$

where N is the total number of Δt clock increments. For turbulent flow where the signal delay spreads over more than one delay increment, then the height of the signal part of the correlogram is divided by the number of delay increments over which the signal delay is spread.

Now assume that the rate of additional uncorrelated pulses on into Channels A and B respectively are λ_a and λ_b. For locations of the cross correlogram other than signal, the correlation function is a flat level with expected value given by NP(1,1) where P(1,1) is the probability of both a 1 in a present sample of Channel A and also a 1 in a delayed sample of Channel B, i.e., for the background locations

$$P_b(1,1) = (\lambda_a\lambda_s + \lambda_b\lambda_s + \lambda_a\lambda_b)\Delta t^2$$

For cases where $\lambda_s << \lambda_a$ or λ_b, as in run 76 for example, $P_b(1,1) \approx \lambda_a\lambda_b$. To demonstrate the numbers practically, we consider run 76:

$$\Delta t = 50\text{x}10^{-9}\ \text{s}$$

$$N = 10^8$$

$$\left.\begin{aligned} \lambda_a &= 15.24\text{x}10^3\ s^{-1} \\ \lambda_b &= 12.76\text{x}10^3\ s^{-1} \end{aligned}\right\}\ *$$

$$\lambda_s = 102$$

$$\text{Background} \simeq (15.24\text{x}10^3)(12.76\text{x}10^3)(50\text{x}10^{-9})^2(10)^8 = 48.6$$

This is to be compared with the run 76 correlator mean value obtained as Background = 50 (see Table 1).

In this example the background level is reasonably low and the experiment agrees with theory. We see that data rate cannot be predicted by measuring the input pulse rates λ_a and λ_b. It must actually be measured with a correlator as was done in the experiments.

4.3 Data Rate Scaling with Laser Power and Optical Efficiency

Figure 14 is a plot of the true data pair rate versus discriminator threshold setting for the Mach 0.9 runs, October 17, 1978. The data is replotted in log-log form in Figure 15. The point from run 72 (50 mv threshold) appears to have been distorted by the single-photon limit wherein continued decrease of threshold produces no additional signal or background pulses. However, due to the statistical range of single photon pulse amplitudes, the limit is not sharply defined. It is just as likely that the statistical variability of the correlogram with high background rates (see run 72 in Appendix) is a cause of error in the estimation of data pair rates for the lower threshold values.

The log-log plots would indicate that within the classical signal regime, the data rate is proportional to the threshold raised to

---

* Actual data measured by the monitor stores of the correlator.

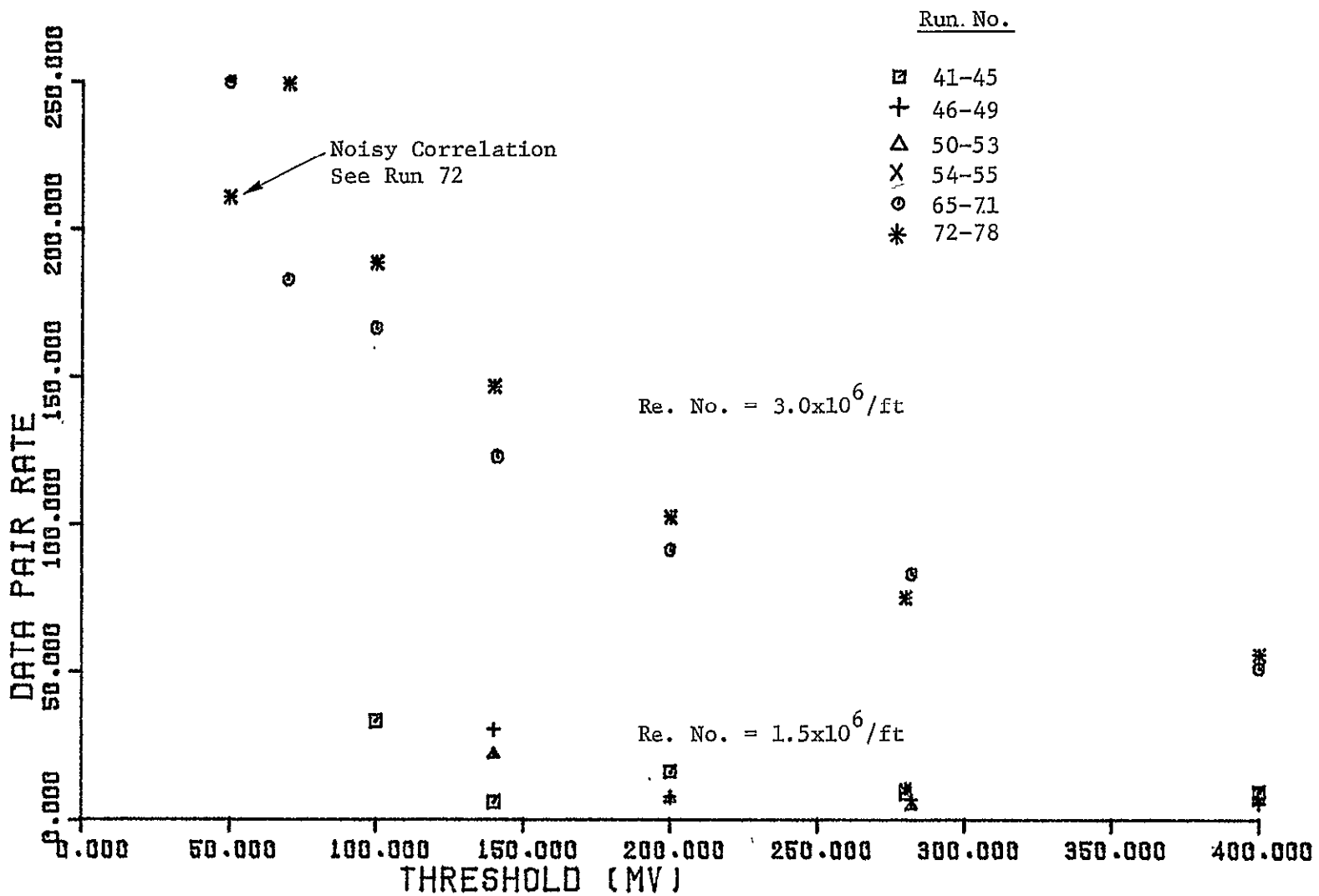

Figure 14. Data Pair Rate Versus Threshold for Mach 0.9 Runs, October 17, 1978.

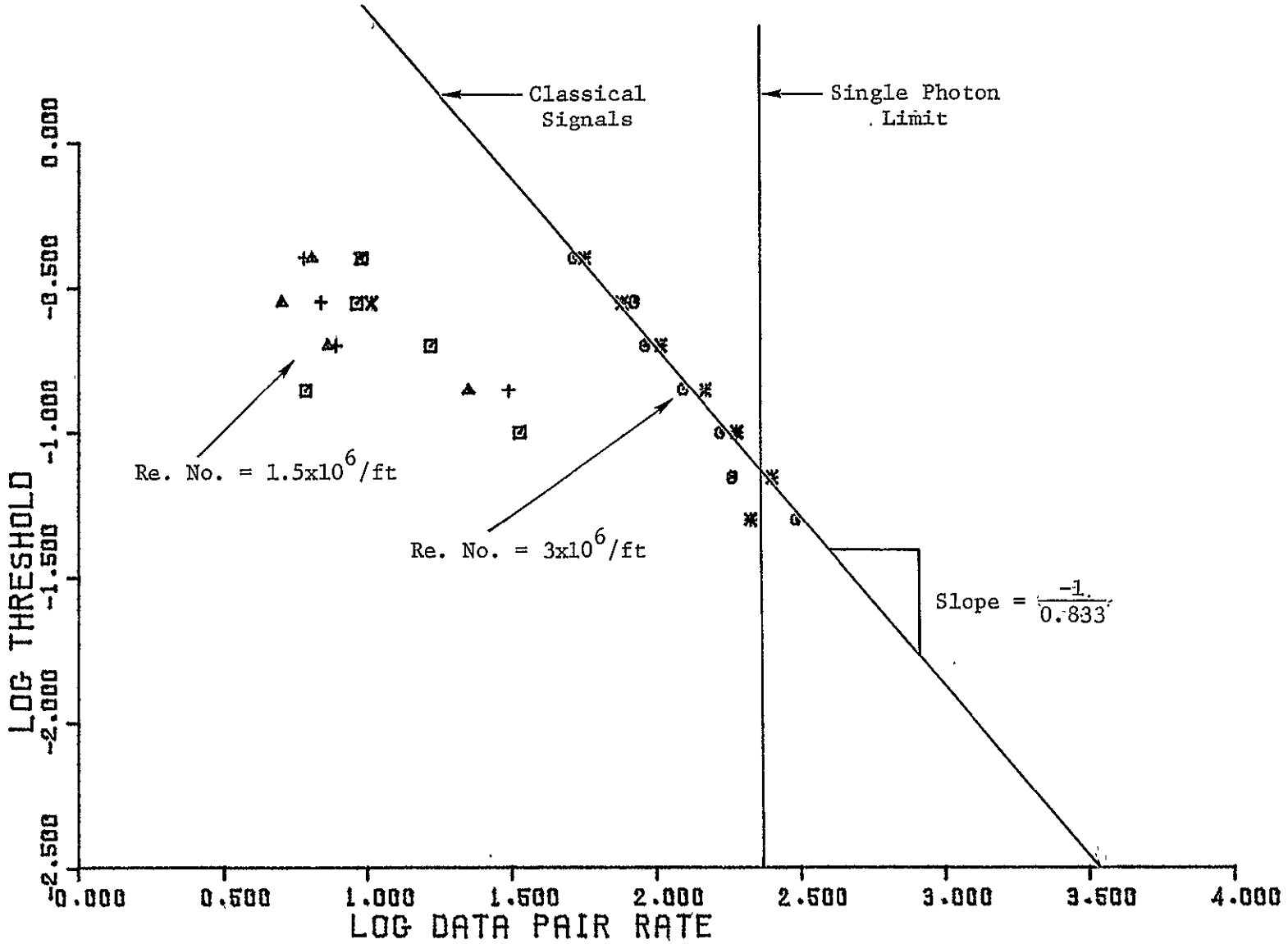

Figure 15. Log-Log Plots of Data Rates from Figure 14.

the minus 0.833 power; or, equivalently, a factor of 10 increase in receiver efficiency or laser power, would result in an increase in data rate by a factor of 7, provided the power law behavior of the scattering coefficients versus size remains the same for the smaller more plentiful particles and that the power law for number density versus size also extrapolated. For practical design purposes we do not really require such an extrapolation. This will become obvious in the next sections as we look at particle size sensitivity simulations and geometric scaling effects.

4.4 System Particle Size Sensitivity Calculations

Figure 16 is a plot of computer calculations of the Mie scattering coefficient for spherical particles with index of refraction $n = 1.4+j0$ at 180 degrees backscatter angle. The diameter range shown is for diameters $0.1\text{x}10^{-6}$ to $1\text{x}10^{-6}$ m. The relative values at $0.25\text{x}10^{-6}$ and $0.5\text{x}10^{-6}$ are seen to be representative (not the bottom or top of the curve oscillations) and to differ in magnitude by about a factor of 10. For many naturally-produced particulate distributions, the number density of submicron sized particles behaves as the inverse of diameter cubed in the range of interest down to $0.1\text{x}10^{-6}$. If such were the case, we would find that an increase of 10 in laser power or a decrease of 10 in detection threshold (classical signals assumed, not down to single photon limit) would decrease the detectable diameter by a factor of 2 which would thus increase the available number by a factor of 8. We do not consider it coincidental that this agrees

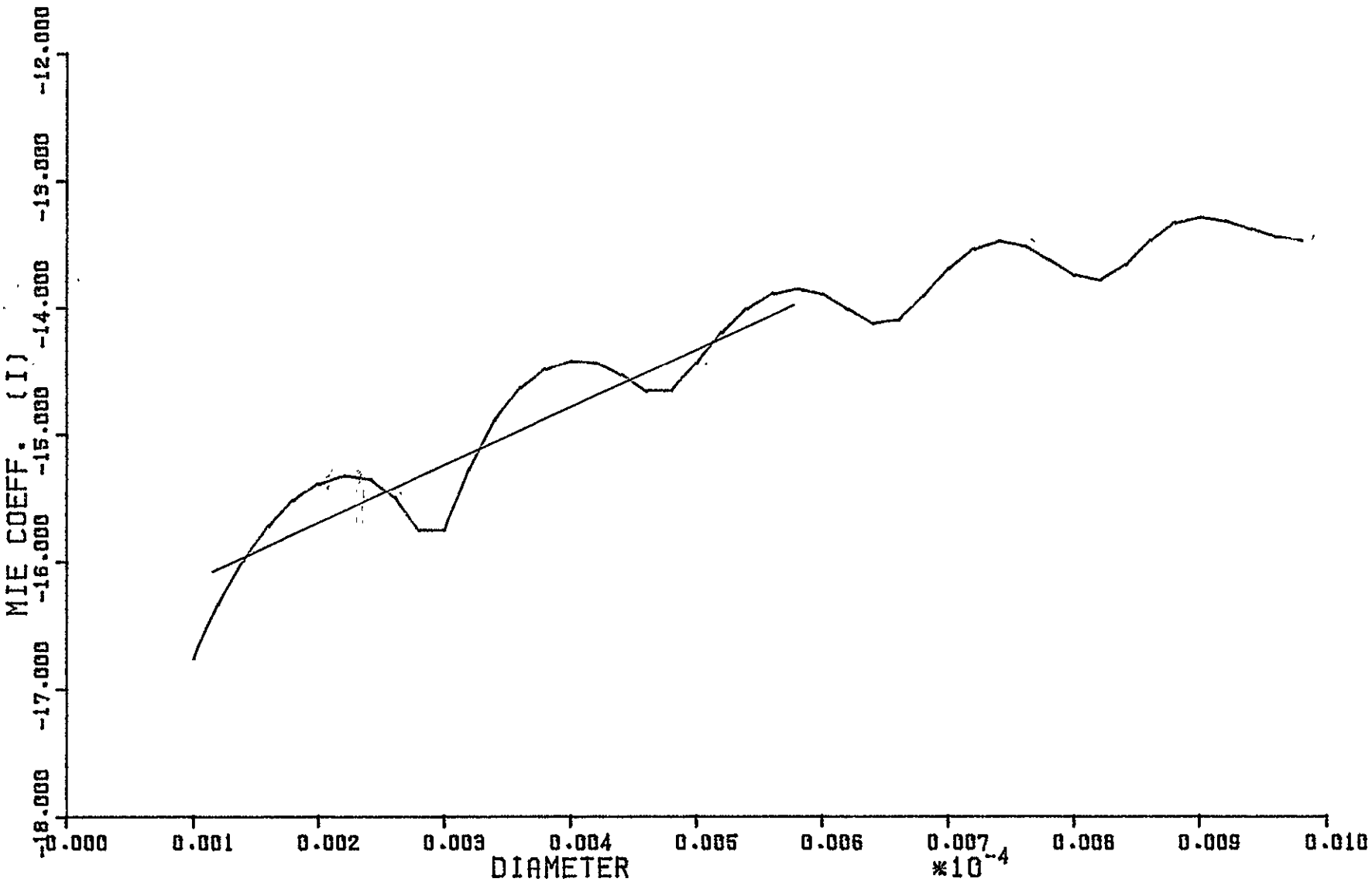

Figure 16. Backscatter Mie Coefficients for Submicron Sized Droplets, n = 1.4+j0.

reasonably well with the experimental data-rate versus log-log slope behavior just described, since our calculations indicate that the particles we were observing went down to about 0.5×10^{-6} m diameter as we now show.

SDL has extensive laser velocimeter simulation software which has been developed over several years for NASA Langley, the U. S. Navy, and the Advanced Research Projects Agency. This software is described briefly in Reference 15. We have used portions of this software and set the 'fringe visibility' and beam intersection angle to zero to simulate signals from a one-spot system. With appropriate inputs, we can use these results to see what the return signals from each of the two spots would look like. The simulation includes random single photoelectron pulse gain statistics for photomultiplier. For purposes of display, we have assumed that four successive, equally spaced scatterers of the same size and composition pass through the center of the scattering volume. We have also assumed a background single photoelectron rate of 5×10^{6}, which is nearly an order of magnitude greater than we encountered experimentally with a 0.135 watt laser. The fixed system parameters for the simulations are shown in Table 2. The variable parameters are discussed along with the results which follow. These simulations were performed prior to the experimental trip to Ames. The simulated range and laser power exceed the experimental parameters of 473 mm and 67 mw/spot in a somewhat compensating manner so that the simulations provide results approximately correct for our experiments.

Table 2. Simulation Parameters.

System	
Wavelength	514.5 nm
Laser Power	0.1 watt/spot
Optical Efficiency	Varied (0.045, 0.30)
Detector Quantum Efficiency	0.15
Transmitted Beam Diameter	25 mm
Range	762 mm
Collecting Lens Diameter	80 mm
Probe Volume Spot Diameter	20.2×10^{-6} m
Single Pulse Duration	50.5×10^{-9} s
Particle	
Velocity	400 m/s
Index of Refraction	1.4-j0
Diameter	Varied (0.25, 0.50×10^{-6} m)
Background Light	5×10^{6} Photoelectrons/s

First let us consider the case where the product of the transmitter and receiver transmission efficiency is 30 percent and the scatterers are 0.5×10^{-6} m diameter. The 30 percent figure includes a 75 percent transmission figure which has been measured and an estimated receiver efficiency of just less than 50 percent. For such conditions, the signals out of the photomultiplier (10 ns rise time) and the signals after low-pass filtering with a Gaussian filter, are shown in Figures 17 and 18. Here the signals are so large that the background single photoelectron pulses are negligible in magnitude and the 'noise' on the classical pulses is negligible in determining the pulse center.

In practice, we observed that about 90 percent of the received light was not focused into the receiver fibers. We had anticipated some such loss, and had run a simulation with an additional receiver factor of 0.15 (which multiplied by 0.3 gives 0.045). The results of that simulation are shown in Figures 19 and 20 where we see that we are reaching the limit of classical threshold detection in the presence of single photoelectron background pulses with statistically varying (Rayleigh distribution assumed) amplitudes. The location of the four signal pulses is the same as in Figures 17 and 18; the other pulses are the background single photoelectron pulses.

In Figures 21 and 22 we show the simulation of 0.25×10^{-6} m diameter particles with the originally assumed 0.3 optical efficiency factor. This is what we would expect with correction of the spherical aberrations which limited the light focused into the fibers in our

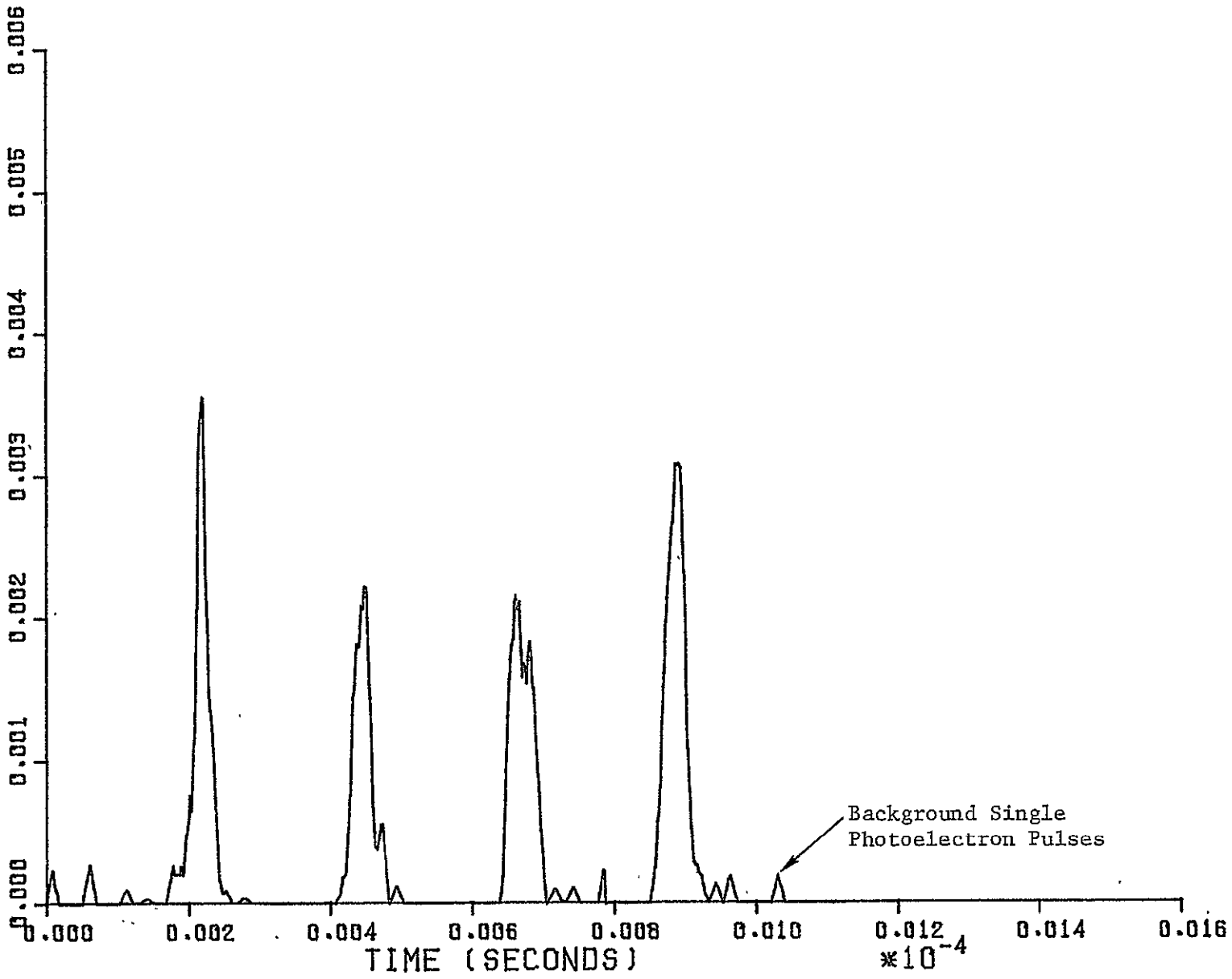

Figure 17. Simulated Photomultiplier Signals, 0.5×10^{-6} m Particles, Optical Efficiency 0.3.

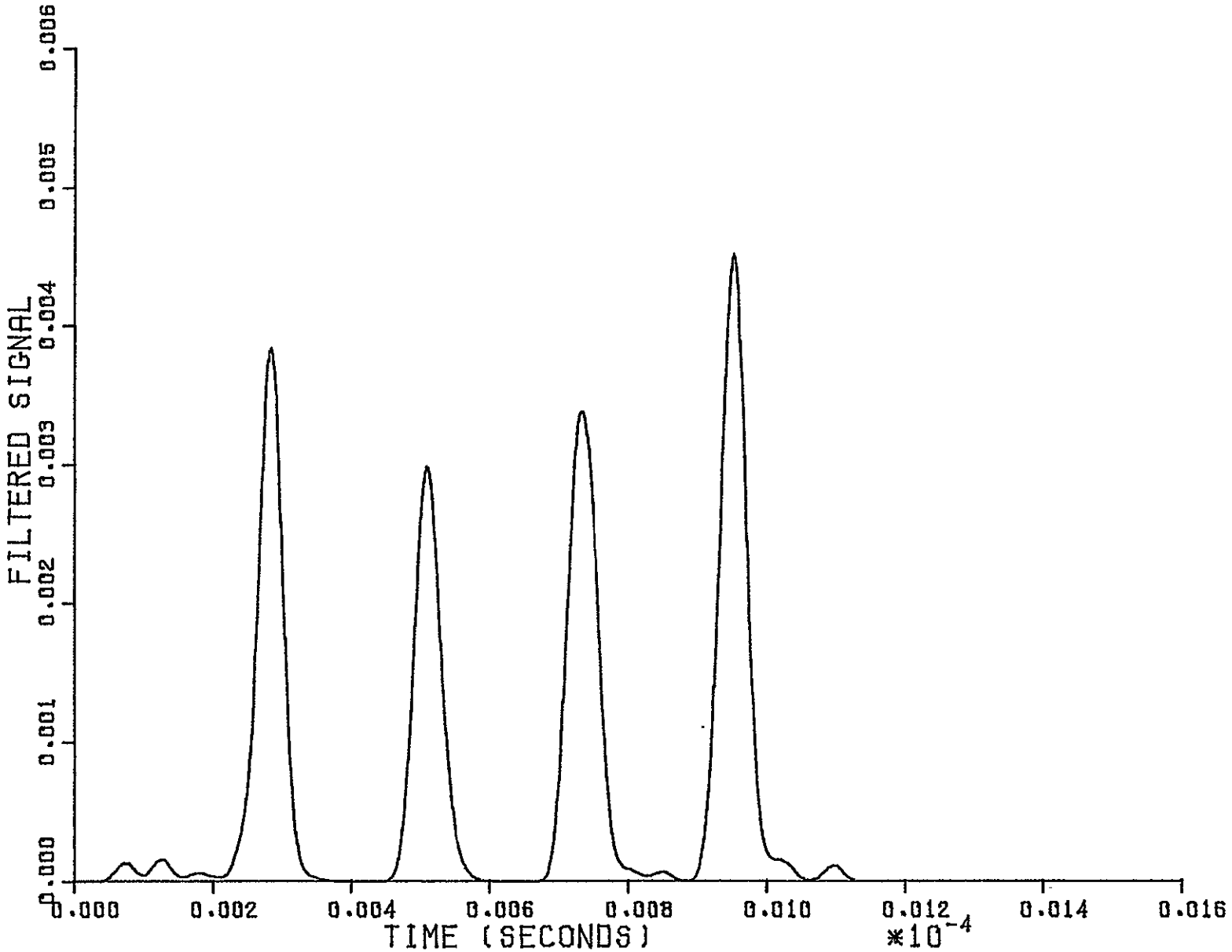

Figure 18. Low-Pass Filtered Signals from Figure 17.

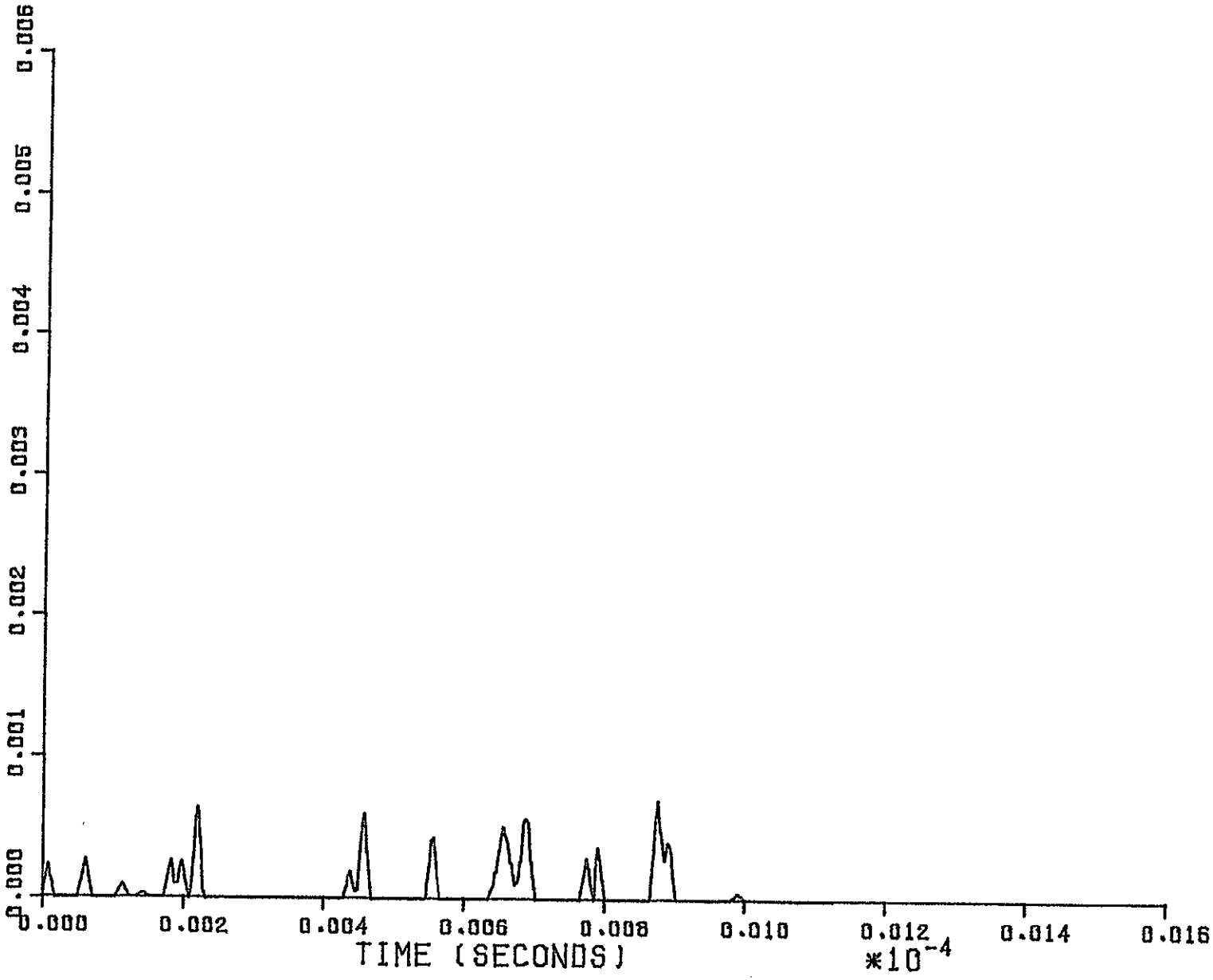

Figure 19. Simulated Signals, 0.5×10^{-6} m Particles, Optical Efficiency 0.3x0.15. (Pulses located at same times as in Figure 17.)

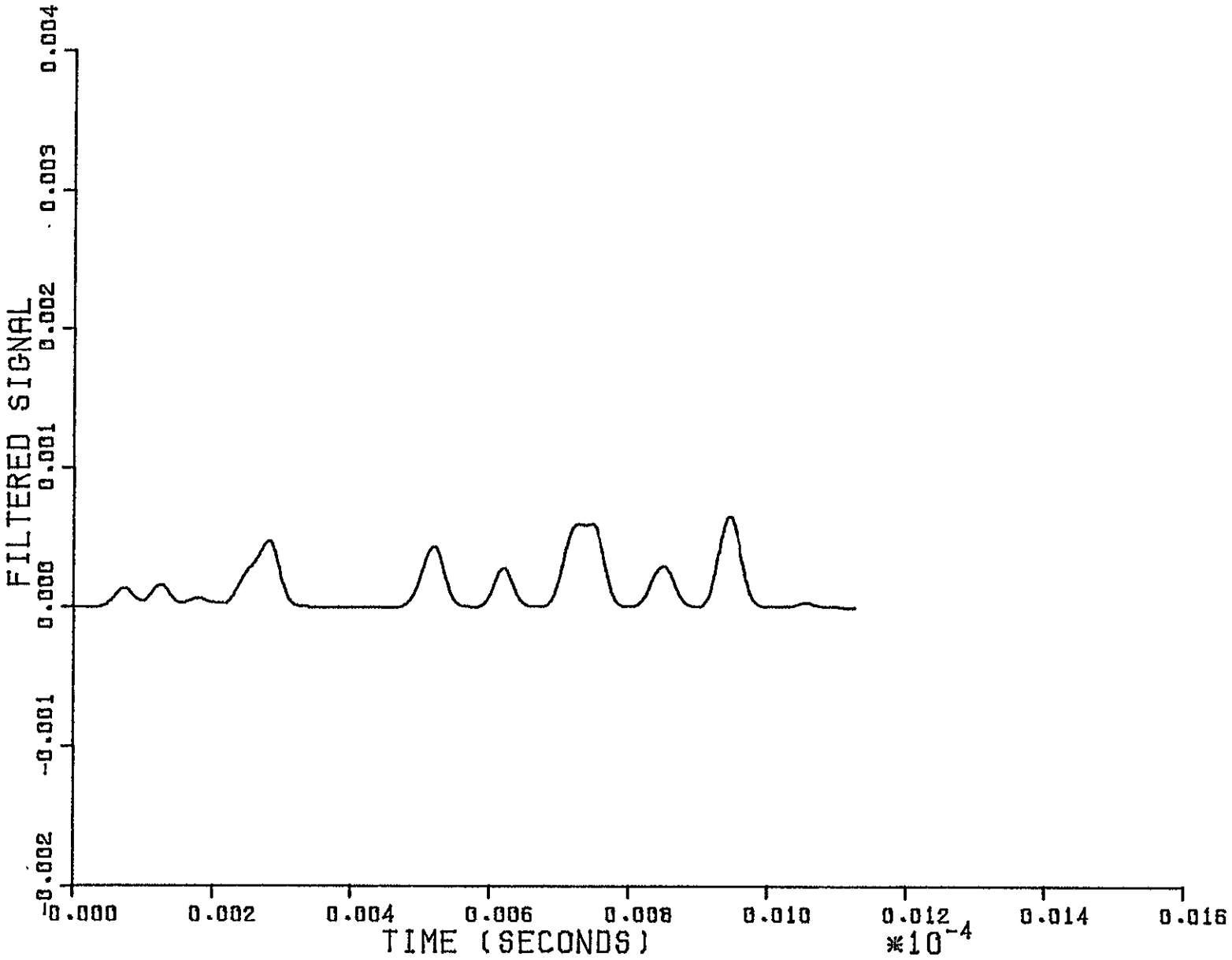

Figure 20. Low-Pass Filtered Signals from Figure 19.

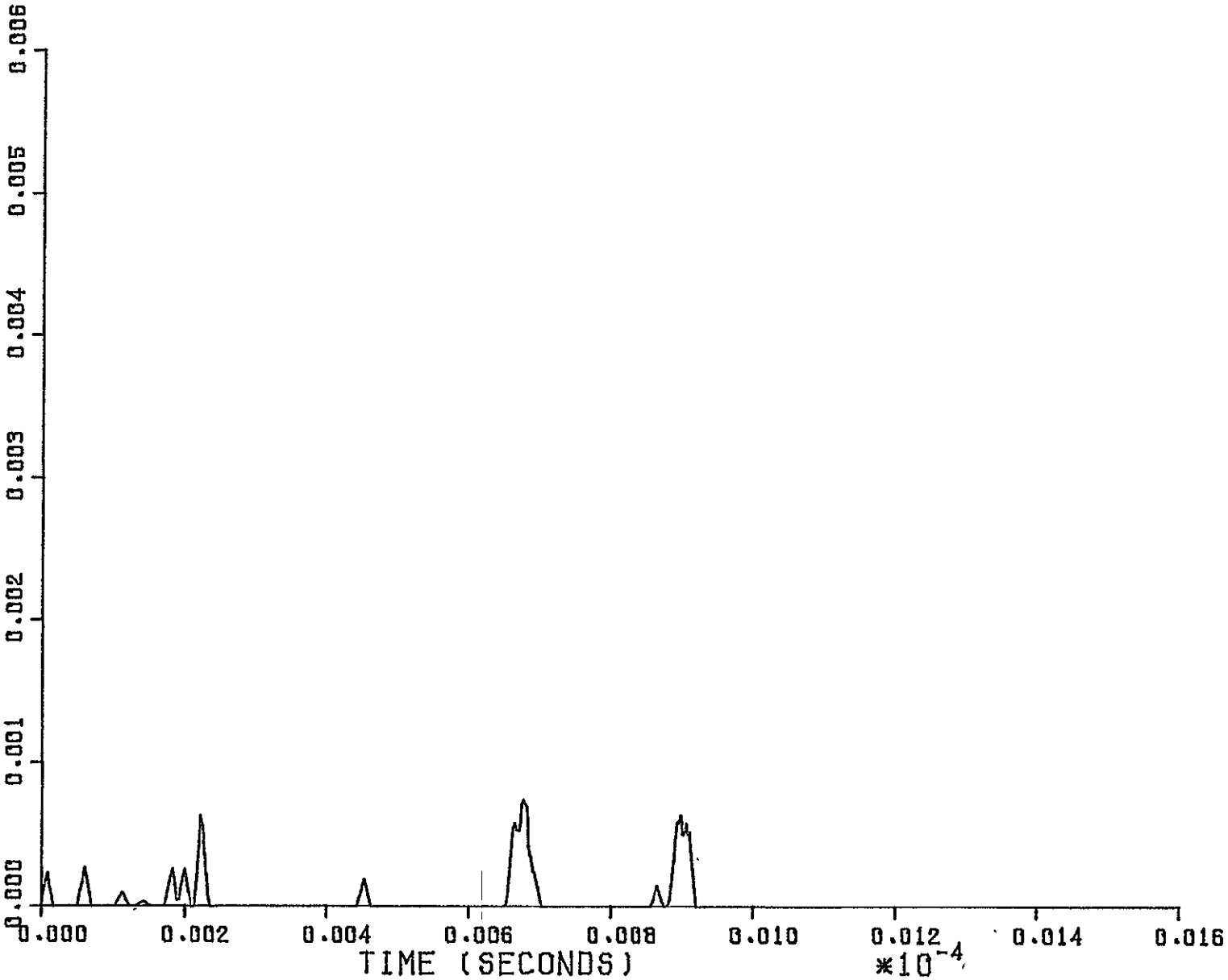

Figure 21. Simulated Photomultiplier Tube Signals, 0.25×10^{-6} m Particles, Optical Efficiency 0.3. (Pulses located at same times as in Figure 17.)

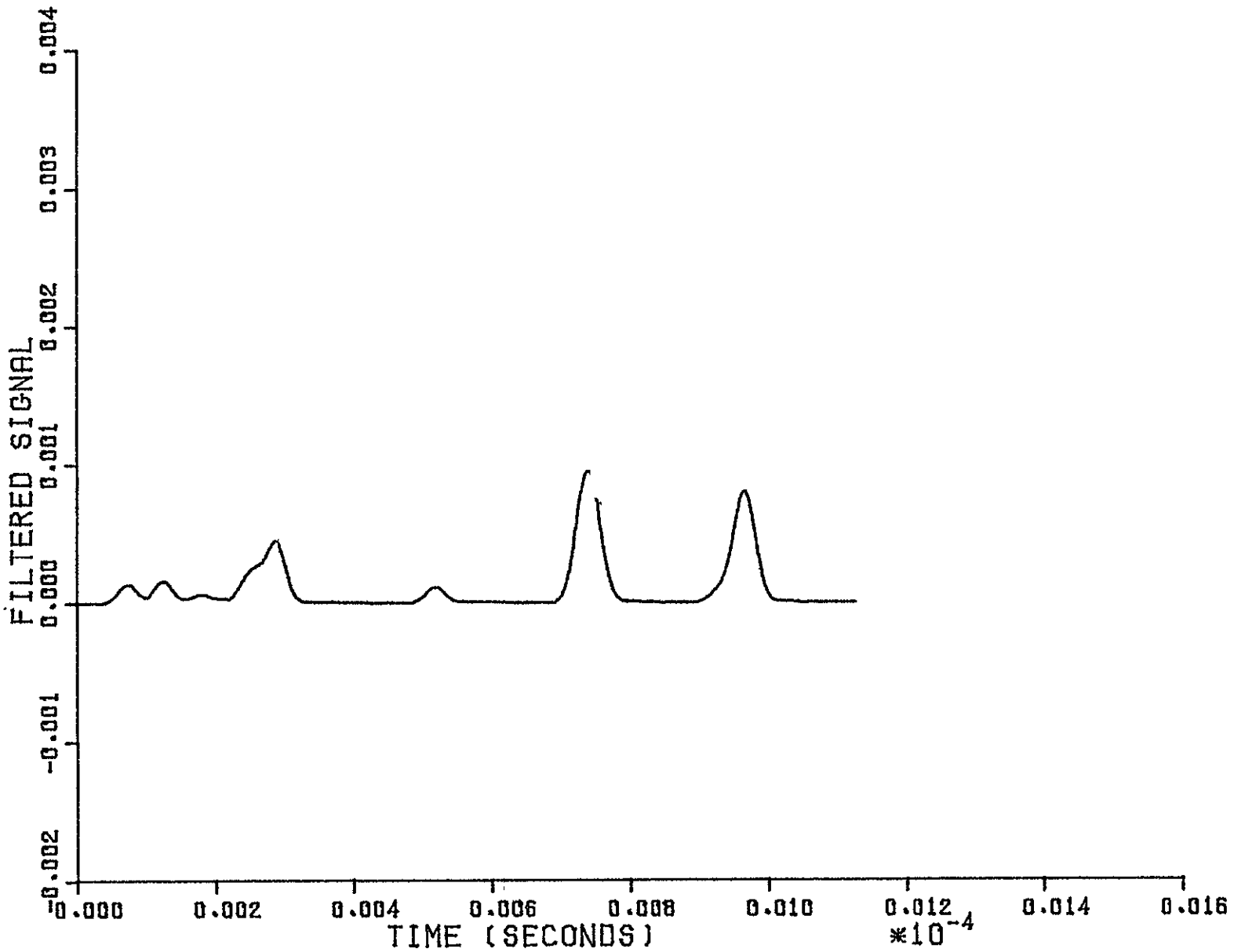

Figure 22. Low-Pass Filtered Signals from Figure 21.

experiments. Now we see that the limit of classical detection is approximately a quarter of a micron diameter with the other system parameters chosen. This is the limit of sensitivity we practically expect once the objective lenses are replaced. Since most natural air contains an abundance of particles at the quarter micron size, we expect no problems without seeding for the standard 0.5 m throw LTA system. In the next section we consider geometric scaling effects for extension of the throw to longer ranges.

4.5 Geometric Scaling Laws

Some of the NASA Ames wind tunnel facilities require velocity measurements at a range of 2 to 3 meters. These ranges are excessive for a system using 80 mm diameter optics if the excellent flare rejection capabilities possible with a transit anemometer system are to be retained. On the other hand, large diffraction-limited optics with large angular aperture become prohibitively difficult to manage. The thickness of the windows can become a major source of aberrations. Final selection must depend on a detailed design tradeoff, but restricting the lens diameters to 15 cm has many advantages in compactness of packaging and ease of use of the system. In this section we briefly explore the effects of geometric size and scale changes on the signals.

First, if the system is scaled in size while maintaining the same f/numbers, then the performance would be unchanged to first order. Thus, by doubling the lens diameters and focal lengths, we should obtain the same performance directly at a 1 meter range as we obtained experimentally at 0.5 m range.

Now we must consider the effect of changing the output lens focal length (and hence f/number). The considerations are identical to those of a fringe mode system. First, if F is the output focal length, then the probe volume length increases as F^2 and the beam waist as F, so that the intercept area A_I illuminated and visible to the receiver increases as F^3. The peak intensity decreases as $1/F^2$ due to the decrease in illumination intensity, and as an additional $1/F^2$ due to the collector solid angle. However, the detectability of a pulse depends on the number of photoelectrons during the spot transit time. The spot transit time is increased in proportion to F. Therefore, the number of photoelectrons per pulse only decreases as $1/F^3$ with range.

It would be interesting if the increase in the rate of particles passing through the probe volume canceled the decrease in signal amplitude, but this doesn't happen. Experimentally, we have seen that the data rate is proportional to threshold raised to the minus 0.833 power. Lowering the threshold is equivalent for data rate of classical signals to raising the detected number of photons per scatterer (inverse relationship). We may thus see that the data rate is proportional to increases in detected number of photons to the 0.833 power.

Combining the above results indicates that the data rate behaves as

$$R = \left(\frac{F}{F_1}\right)^3 \left[\left(\frac{F_1}{F}\right)^3 \frac{P}{P_1}\right]^{0.833}$$

where F_1 is the normalizing (experimentally used) focal length and P is the laser power normalized by that used experimentally P_1. The formula is only valid for small excursions of F from F_1 and P from P_1 because the power law behavior of the Mie scattering coefficients and the particle size distributions will change at considerably smaller ($<0.5 \times 10^{-6}$ m) or larger (1×10^{-6} m) particles.

For a conservative engineering design which keeps the small particle sensitivity instead of getting the data rate back because the large probe volume cross section intercepts more larger particles, we recommend an increase in laser power and/or detection efficiency to compensate for the $1/F^3$ effect of a longer focus lens. The larger probe cross section will then just provide a higher data rate which would prove useful comfort margin for other tunnel conditions and higher turbulence. Fortunately, a factor of approximately 8 to 10 increase in detection efficiency is expected due to the use of higher performance lenses without the losses due to aberration. Thus, any extra laser power will be simply for design margin and higher performance in more difficult measurements.

5.0 SUMMARY AND DESIGN RECOMMENDATIONS

1. A laser transit anemometer (LTA) has been shown to be capable of 0.15 percent precision of backscatter mean-flow measurements with unseeded transonic flow in the NASA Ames 6' x 6' wind tunnel at a range of 48 cm, with an 80 mm diameter lens and a 0.135 watt argon laser operating at 514.5 nm.

2. Analysis and simulation shows that purely classical mode pulse detection is wasteful of available data which may be extracted by pulse correlation techniques; however, in practical background and flare conditions with coaxial argon laser systems, single-photon correlation detection is also not optimum due to the statistical variance added by the background. The optimum detection is thus a semi-classical detection system with the detection threshold set at a multiple-photon level. Correlation detection is required for optimum sensitivity, but 5 to 10 ns precision is desirable for the measurement of turbulence intensities at values of less than 0.5 percent for transonic flows.

3. Scaling equations indicate that a superior system with a range of 2 to 3 meters is possible using high-performance 15 to 20 cm diameter lenses and a 400 mw argon laser. Higher power may be detrimental to system reliability, would incur Class IV safety precautions, and is not recommended. The engineering of such a system is a natural extension of the present SDL LTA system. Computer simulation indicates that the sensitivity of the experimental system and, hence, the scaled

2 meter system would be for particles less than 0.5×10^{-6} m in diameter. Operation of a system at 3 meters would degrade the system performance, but good data should still be obtained.

6.0 REFERENCES

1. Johnson, D. A., "Turbulence Measurements in a Mach 2.9 Boundary Layer Using Laser Velocimetry," AIAA Journal, 12, No. 2, pp. 711-714, May 1974.

2. Johnson, D. A. and Rose, W. C., "Laser Velocimeter and Hot Wire Anemometer Comparison in a Supersonic Boundary Layer," AIAA Journal, 13, pp. 512-515, April 1975.

3. Barnett, D. O. and Giel, T. V., "Laser Velocimeter Measurements in Moderately Heated Jet Flows," AEDC-TR-76-156, April 1972.

4. Johnson, D. A., Bachalo, W. D., and Moddaress, D., "Laser Velocimetry Applied to Transonic and Supersonic Aerodynamics," in AGARD Conference Proceedings No. 193 on Applications of Non-Intrusive Instrumentation in Fluid Flow Research, published September 1976.

5. Mayo, W. T., Jr., "Modeling Laser Velocimeter Signals as Triply Stochastic Poisson Processes," in Proceedings of Minnesota Symposium on Laser Anemometry, held October 22-24, 1975.

6. Mayo, W. T., Jr., "Digital Photon Correlation Data Processing Techniques," AEDC-TR-76-81, July 1976.

7. Schodl, R., "On the Extension of the Range of Applicability of LDA by Means of the Laser-Dual-Focus (L-2-F) Technique," Proceedings of the LDA-Symposium Copenhagen, 1975.

8. Cummins, H. Z. and Pike, E. R., Photon Correlation Spectroscopy and Laser Velocimetry, Plenum Press, New York, 1977.

9. Mayo, W. T., Jr., "Study of Photon Correlation Techniques for Processing of Laser Velocimeter Signals," NASA CR-2780, February 1977. (A design study. Correlator hardware delivered in succeeding contract, but no wide distribution reports available.)

10. Abbiss, J. B., Chubb, T. W., and Pike, E. R., "Supersonic Flow Investigations with a Photon Correlator, "Proceedings of the Second International Workshop on Laser Velocimetry, Purdue University, LaFayette, Indiana, March 22-29, 1974.

11. Smart, A. E., "Special Problems of Laser Anemometry in Difficult Applications," AGARD Lecture Series No. 90, 25-26 August 1977.

12. Smart, A. E., "Transit Anemometer Trials at the Cambridge Whittle Laboratory," presented at meeting on Photon Correlation Techniques in Fluid Mechanics, Churchill College, Cambridge, England, 6-7 April 1977.

13. Smart, A. E., "Data Retrieval in Laser Anemometry by Digital Correlation," Third International Workshop on Laser Velocimetry, Purdue University, LaFayette, Indiana, 11-13 July 1978.

14. Smart, A. E., "Laser Anemometry Close to Walls," Dynamic Flow Conference 1978, Baltimore, Maryland, 18-21 September 1978.

15. Mayo, W. T., Jr., "Ocean Laser Velocimetry Systems: Signal Processing Accuracy by Simulation," Third International Workshop on Laser Velocimetry, Purdue University, LaFayette, Indiana, 11-13 July, 1978.

16. Smart, A. E. and Mayo, W. T., Jr., "Applications of Laser Anemometry to High Reynolds Number Flows," Conference on Photon Correlation Techniques in Fluid Mechanics, Stockholm, Sweden, 14-16 June 1978.

17. Mayo, W. T., Jr., "A Two Component LDV System with Photon Counting for the NASA Langley V/STOL Tunnel: Preliminary Design Study," Final Report for NASA Contract NAS1-13737, October 12, 1976.

18. Mayo, W. T., Jr., "Fringe LV Photon Correlation Interpretation Program Software Manual," Final Report for NASA Contract NAS1-14963, 11 November 1977.

19. Mayo, W. T., Jr. "Photon Counting Processing for Laser Velocimetry," Applied Optics, 16, p. 1157, May 1977.

20. Mayo, W. T., Jr., "Photon Counting Frequency Discriminator for LDV Systems," from Photon Correlation Spectroscopy and Velocimetry edited by H. Z. Cummins and E. R. Pike, Plenum Publishing Corporation, 1977.

21. Mayo, W. T., Jr., "Study of Photon Correlation Techniques for Processing of Laser Velocimeter Signals," NASA CR-2780, February 1977.

22. Mayo, W. T., Jr. "Advanced Photon Counting Processor for Low-Level LDV Signals," Final Report for NASA Contract NAS1-14384, October 5, 1976.

APPENDIX

Plots of the Correlograms from Runs October 17, 1978.

All Plots Normalized to Peak Value.

RN = 1.5×10^6, M = 1.1, A = 1900 v, B = 1980 v

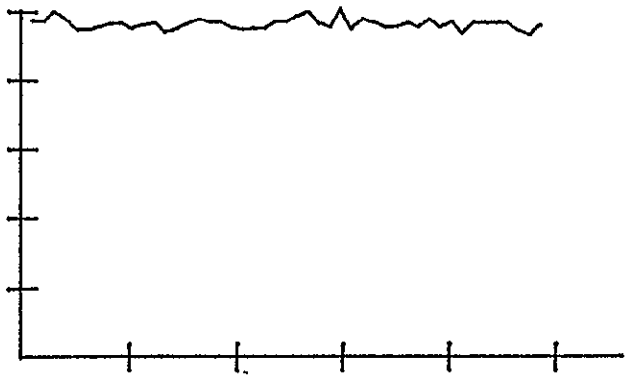

RUN 1 PEAK= 5712 50 mv

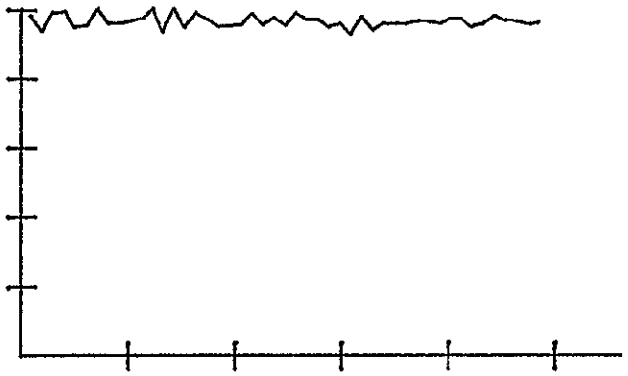

RUN 2 PEAK= 4187 70 mv

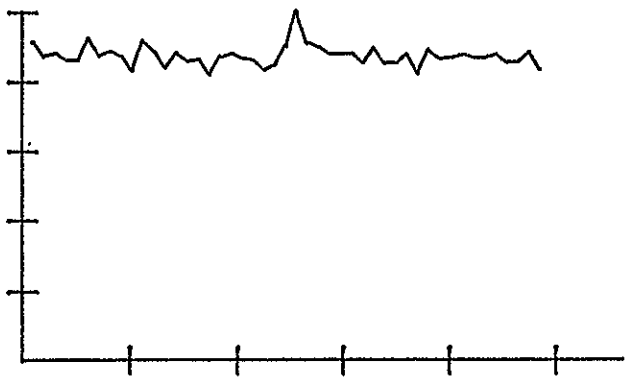

RUN 3 PEAK= 2754 160 mv

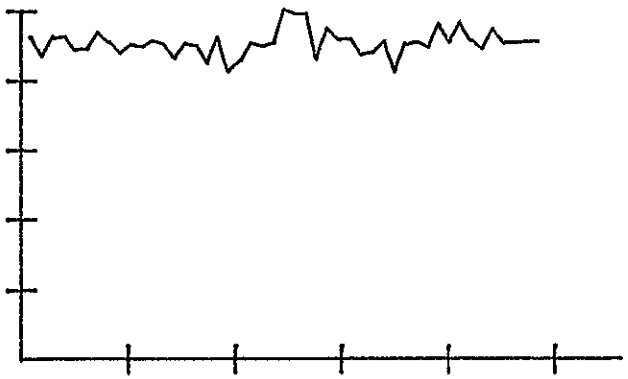

RUN 4 PEAK= 894 140 mv

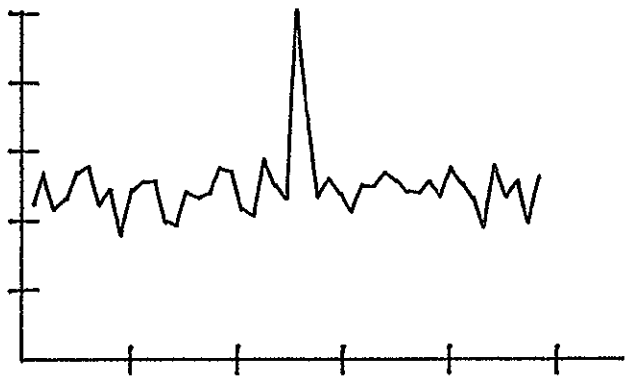

RUN 5 PEAK= 163 200 mv

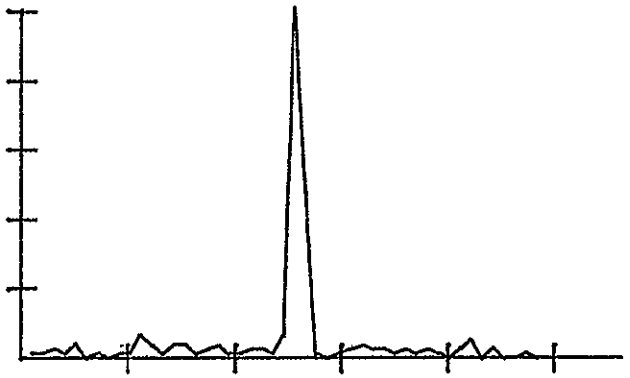

RUN 6 PEAK= 82 282 mv

M → 1.1, A = 1917 v, B = 1900 v

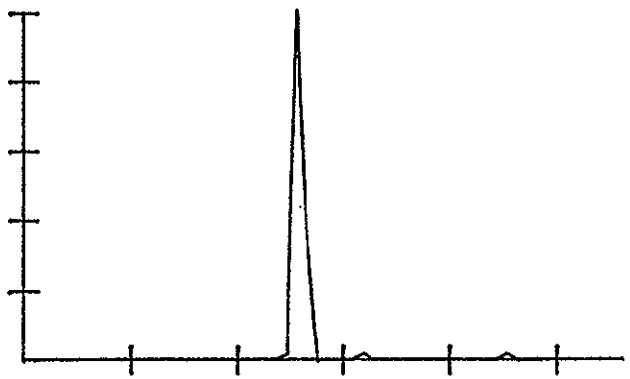

RUN 7 PEAK= 65 400 mv

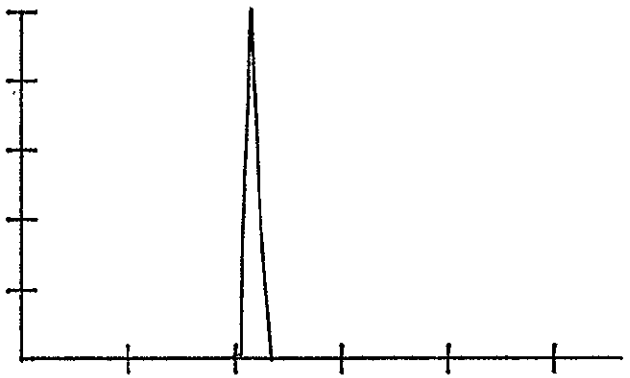

RUN 8 PEAK= 78 400 mv

M = 1.1, A = 1917 v, B = 1900 v

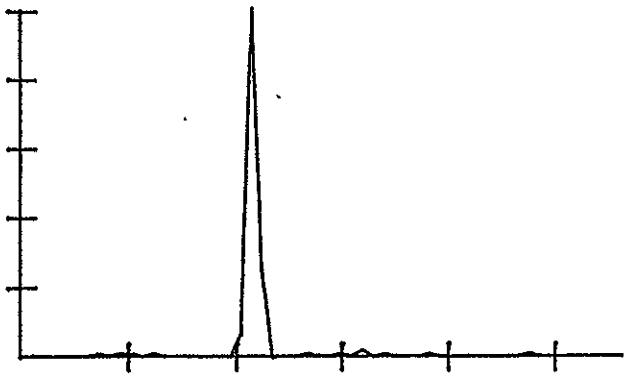

RUN 9 PEAK= 135 282 mv

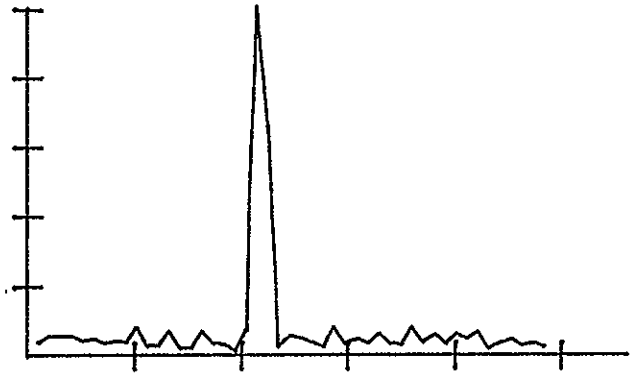

RUN 10 PEAK= 172 200 mv

M = 1.1

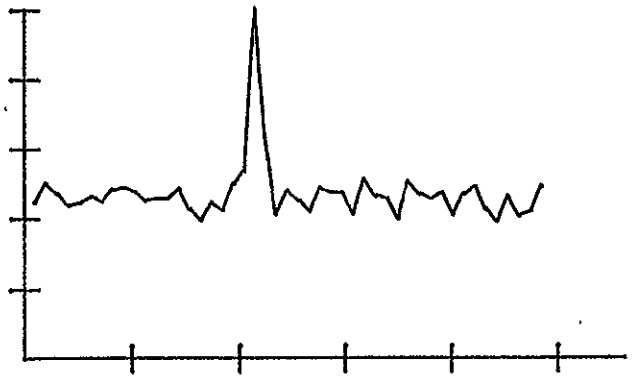

RUN 11 PEAK= 459 140 mv

M = 1.1

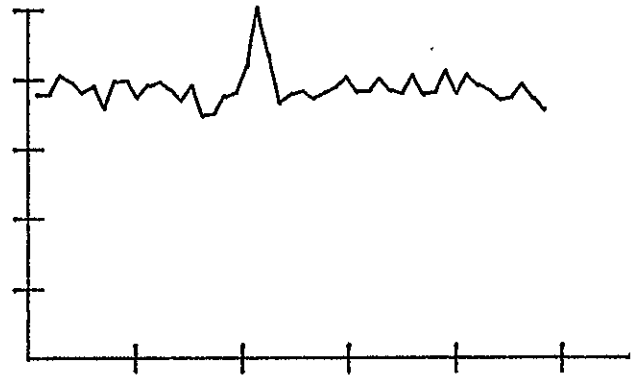

RUN 12 PEAK= 1491 100 mv

A = 1917 v, B = 1900 v

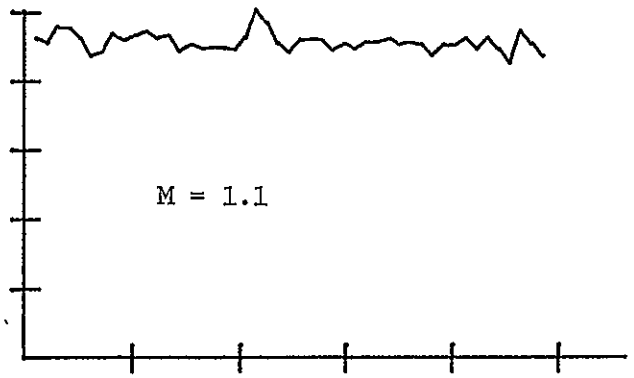

RUN 13 PEAK= 3029 70 mv

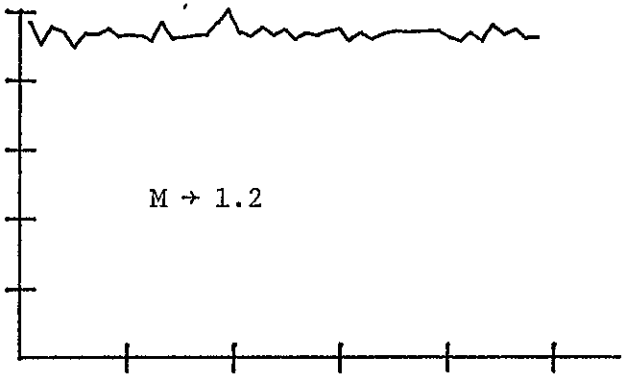

RUN 14 PEAK= 4818 50 mv

RN = 1.5×10^6, M1.2 → M1.3, A → 1900 v, B → 1960 v

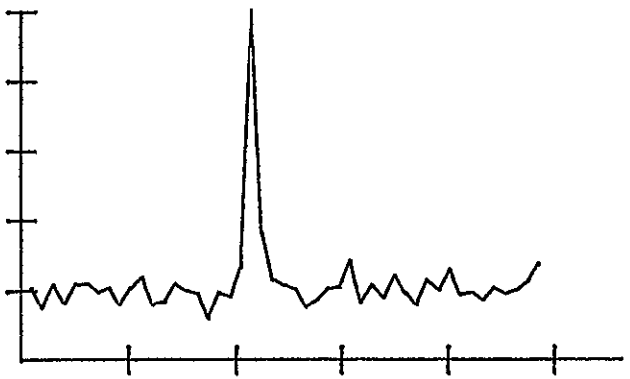

RUN 15 PEAK= 231 200 mv

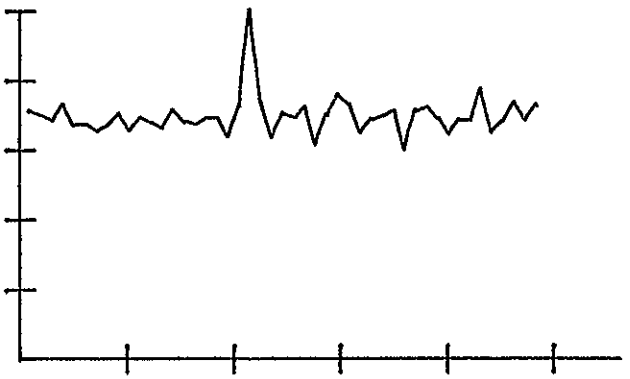

RUN 16 PEAK= 913 140 mv

A = 1900 v, B = 1960 v

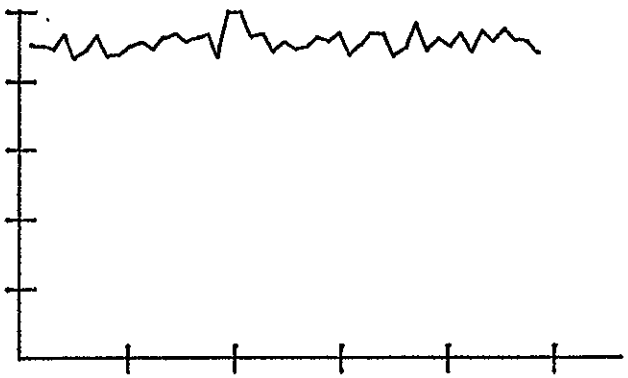

RUN 17 PEAK= 2234 100 mv

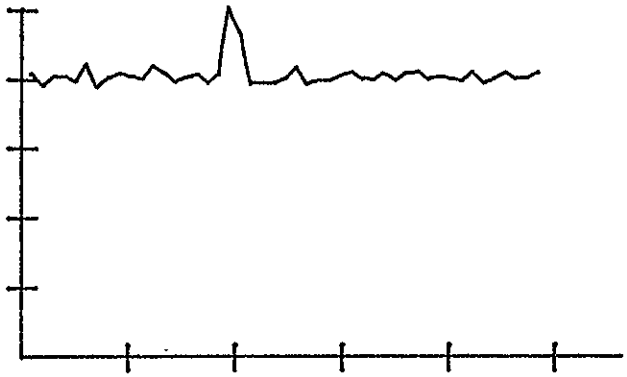

RUN 18 PEAK= 4697 70 mv

Jump back to high thresholds

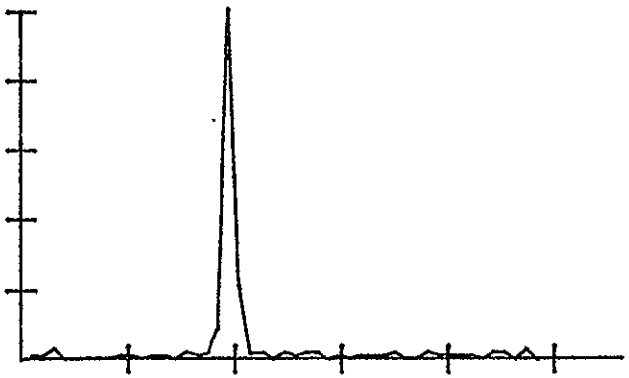

RUN 19 PEAK= 117 282 mv

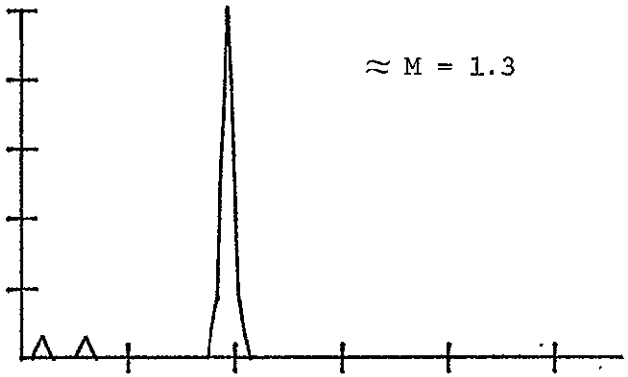

RUN 20 PEAK= 18 400 mv

RN = 1.5×10^6, Tunnel going from M1.3 → 1.6 while we took data

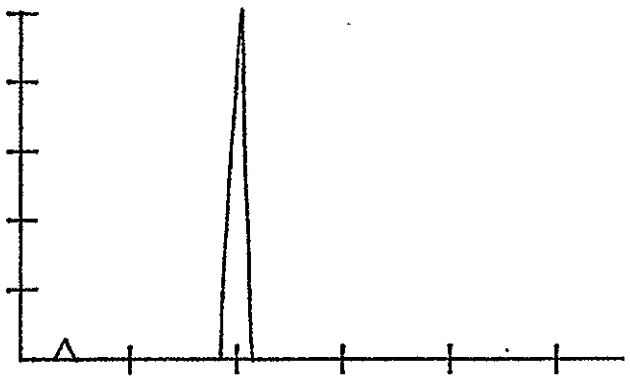

RUN 21 PEAK= 20 400 mv

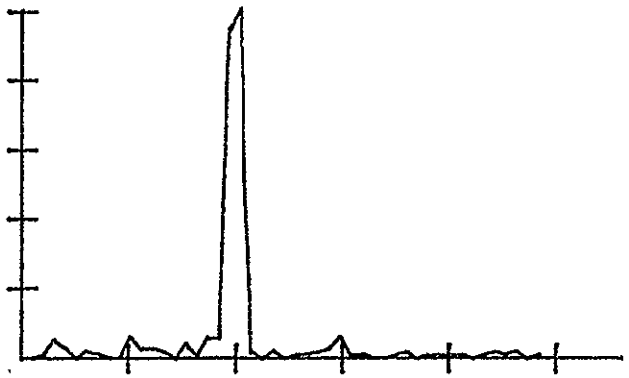

RUN 22 PEAK= 106 282 mv

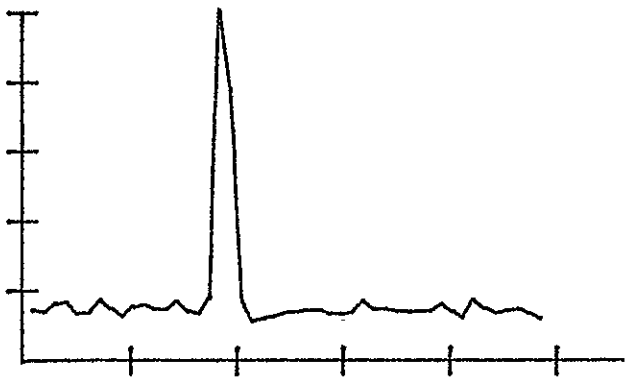

RUN 23 PEAK= 1086 200 mv

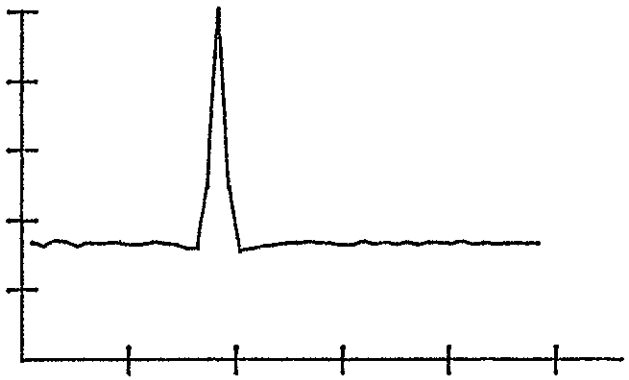

RUN 24 PEAK= 48240 140 mv

Fog came with high Mach number;
signal = rubbish after that

Errors in transfer

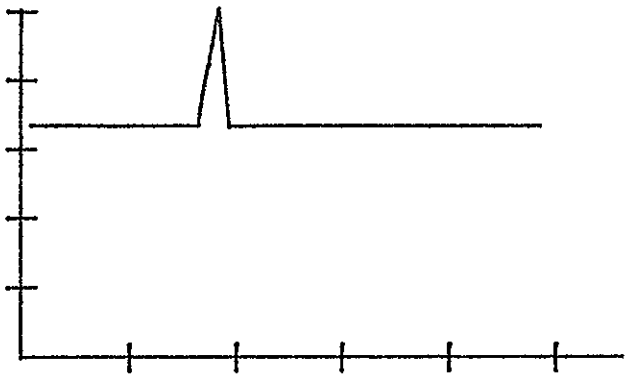

RUN 25 PEAK= 101077328 2.45 mv

RN = 1.5×10^6, M = 1.6, Heavy fog

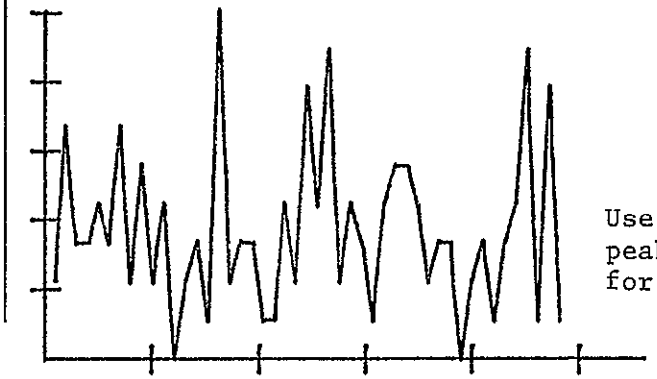

Use peak for v

RUN 26 PEAK= 9 400 mv

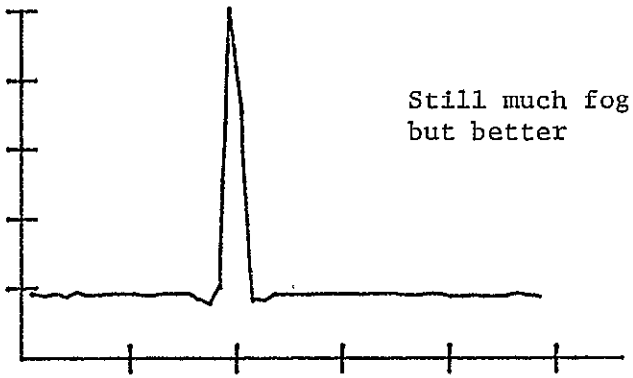

Still much fog but better

RUN 27 PEAK= 10348 400 mv

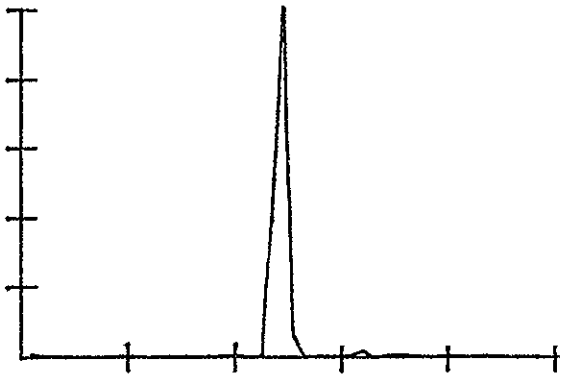

RUN 28 PEAK= 299 282 mv

Fog became (apparently) larger particles and then went away during this time. (Compare runs 27 and 32.1 at same threshold.) Tunnel slowing down in these runs.

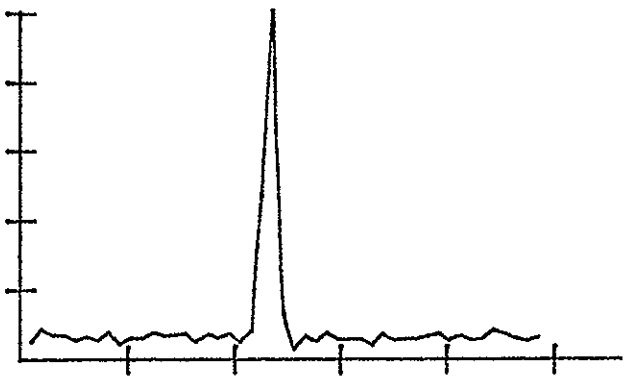

RUN 29 PEAK= 569 200 mv

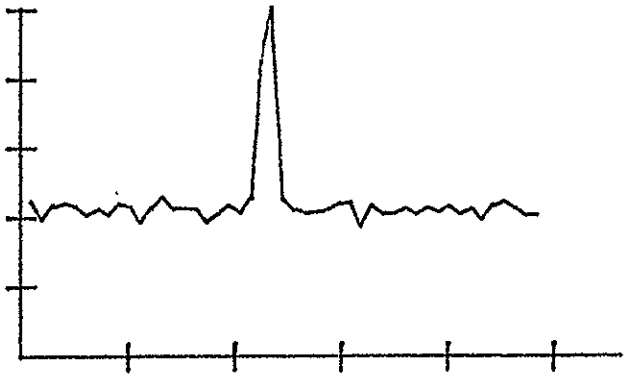

RUN 30 PEAK= 1360 140 mv

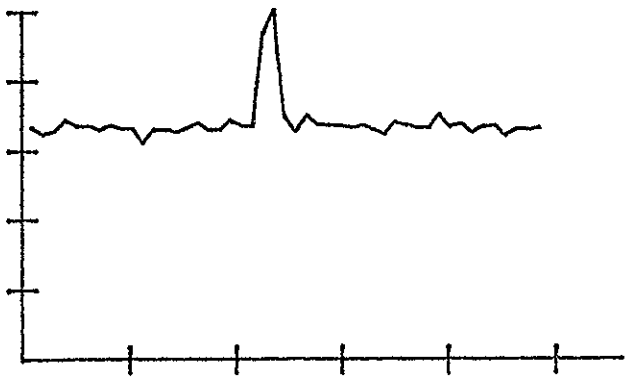

RUN 31 PEAK= 3098 100 mv

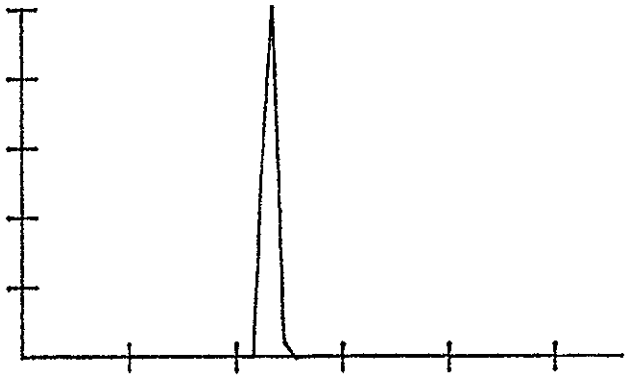

RUN 32.1 PEAK= 235 400 mv

Going to RN = 1.5×10^6, M = 0.9

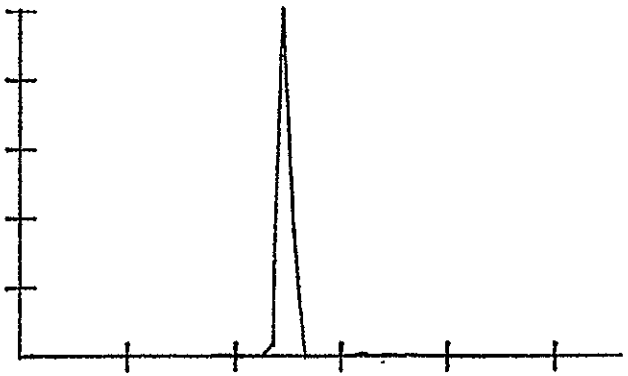

RUN 32.2 PEAK= 259 400 mv

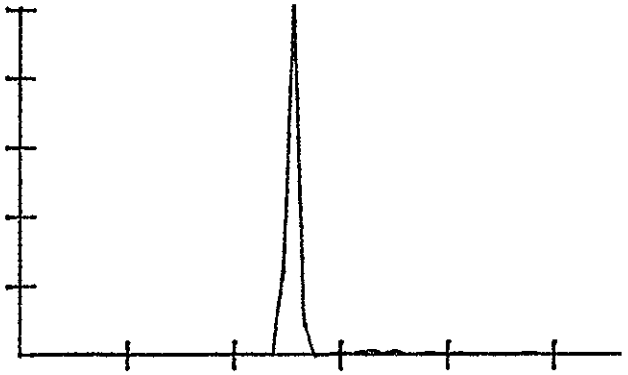

RUN 33 PEAK= 404 280 mv

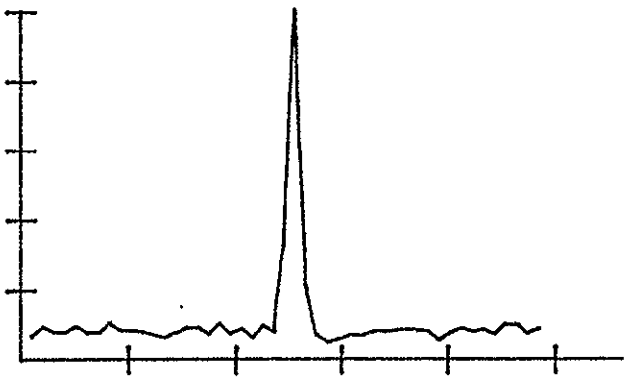

RUN 34 PEAK= 540 200 mv

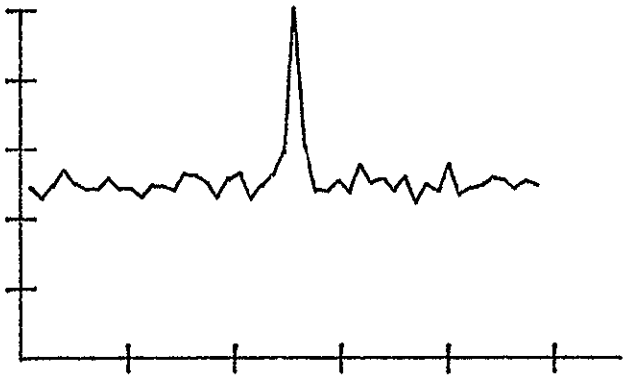

RUN 36 PEAK= 1216 141 mv

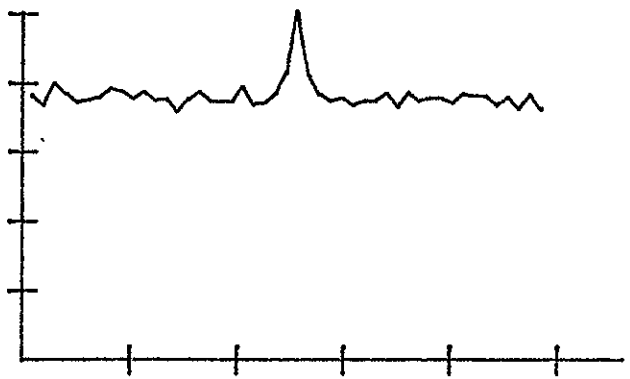

RUN 36 PEAK= 2782 100 mv

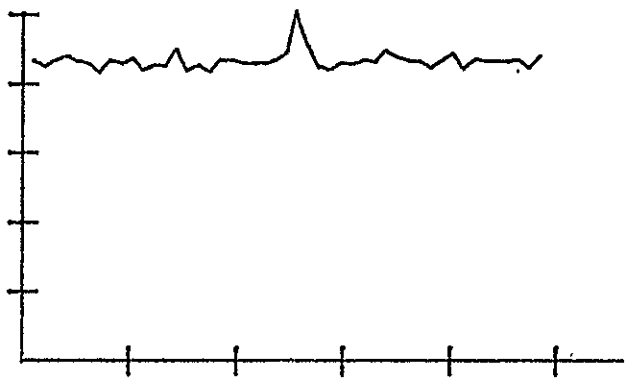

RUN 37 PEAK= 4470 70 mv

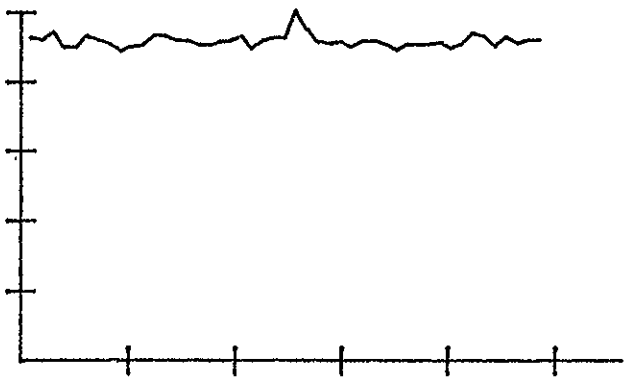

RUN 38 PEAK= 5879 50 mv

RN = 1.5×10^6, M = 0.9

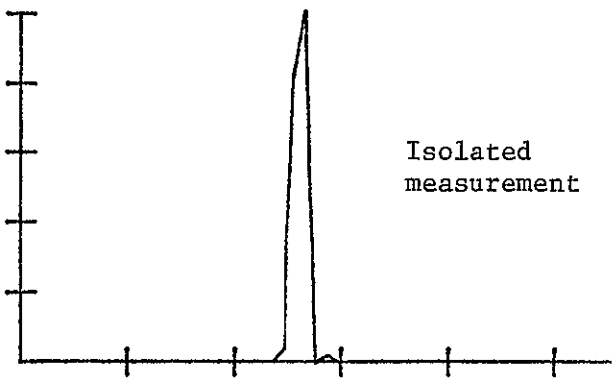

RUN 39 PEAK= 60 400 mv

Repeat, RN = 1.5×10^6, M = 0.9

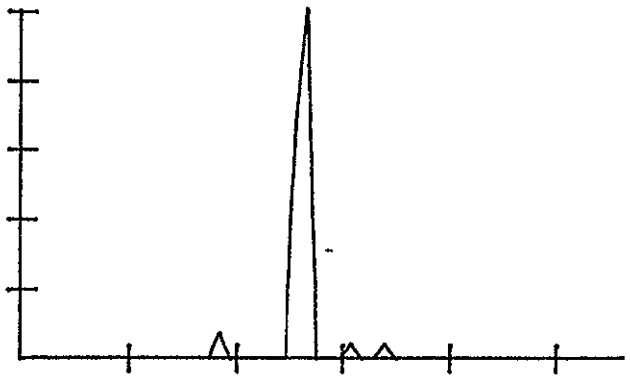

RUN 41 PEAK= 29 400 mv

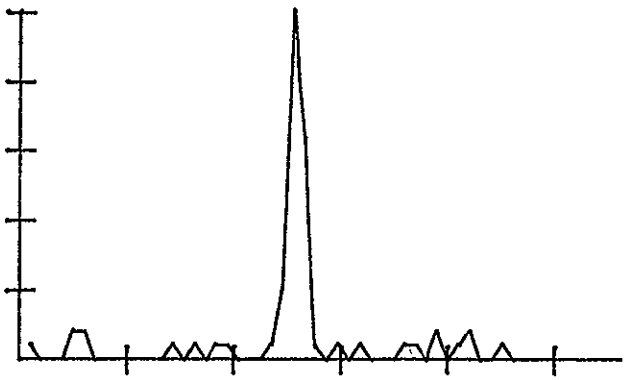

RUN 42 PEAK= 25 280 mv

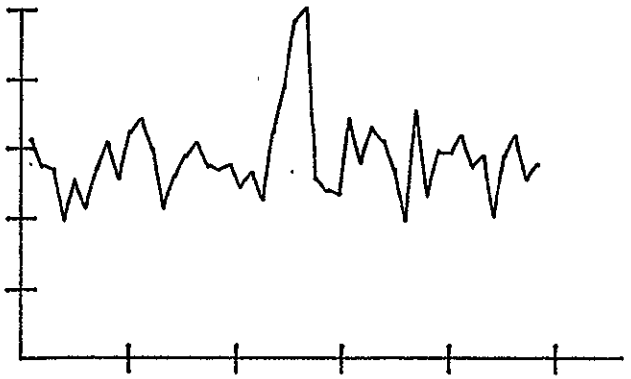

RUN 43 PEAK= 85 200 mv

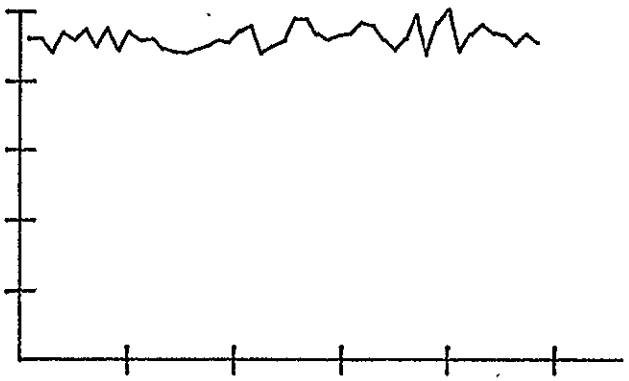

RUN 44 PEAK= 670 140 mv

Record Data, then rerun M = 0.9

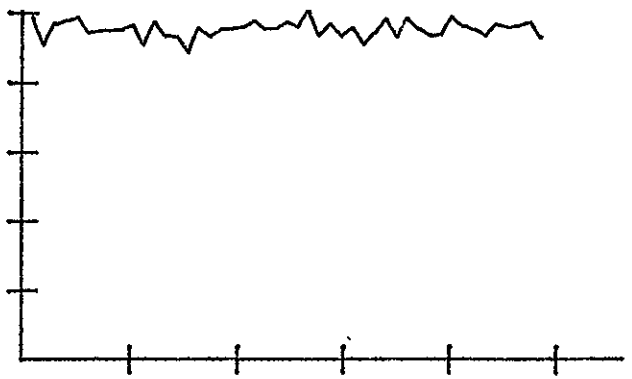

RUN 45 PEAK= 2179 100 mv

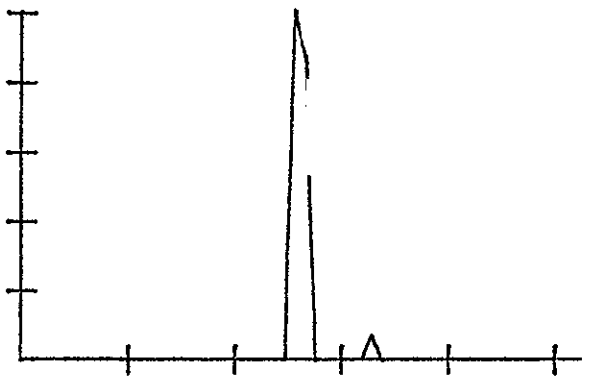

RUN 46 PEAK= 16 400 mv

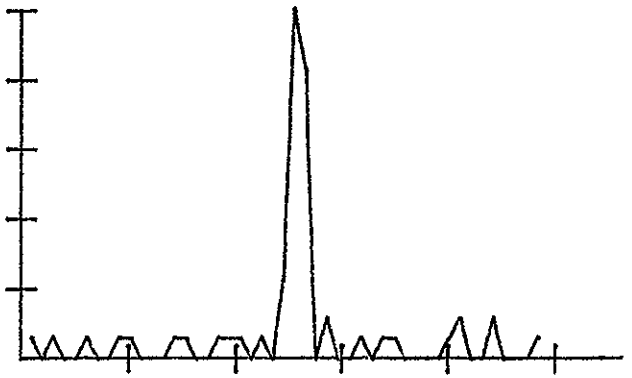

RUN 47 PEAK= 18 282 mv

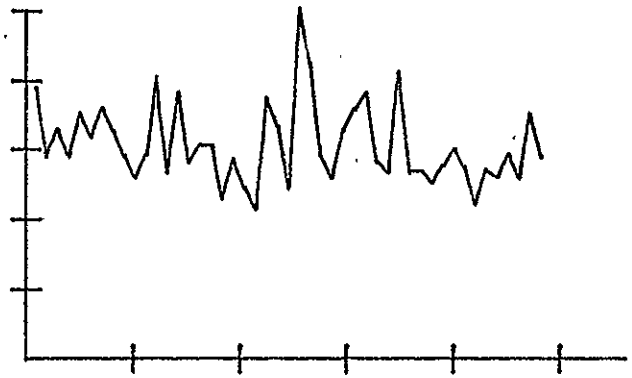

RUN 48 PEAK= 67 200 mv

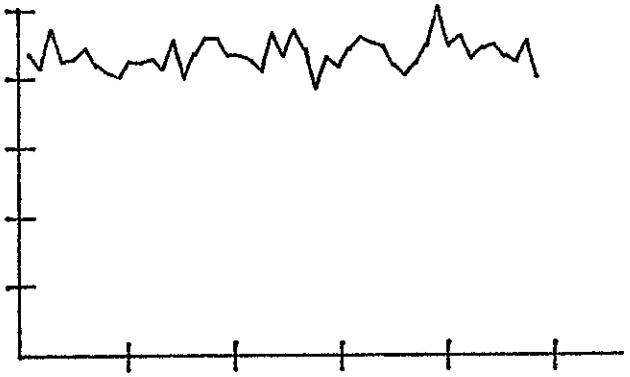

RUN 49 PEAK= 660 140 mv

Rerun on M = 0.9

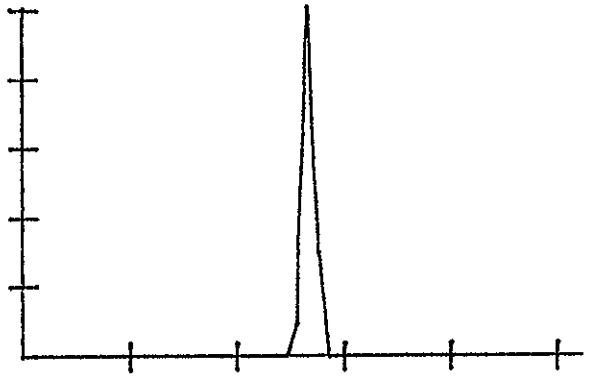

RUN 50 PEAK= 23 400 mv

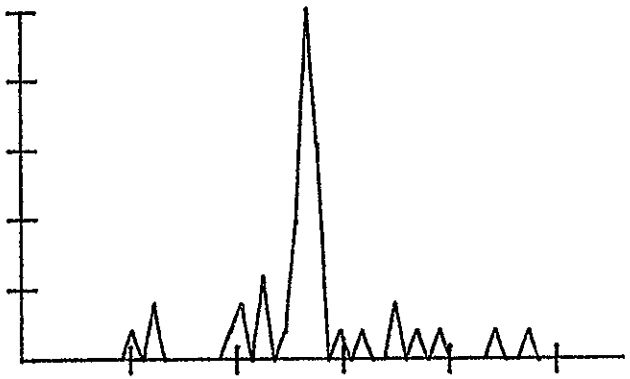

RUN 51 PEAK= 13 282 mv

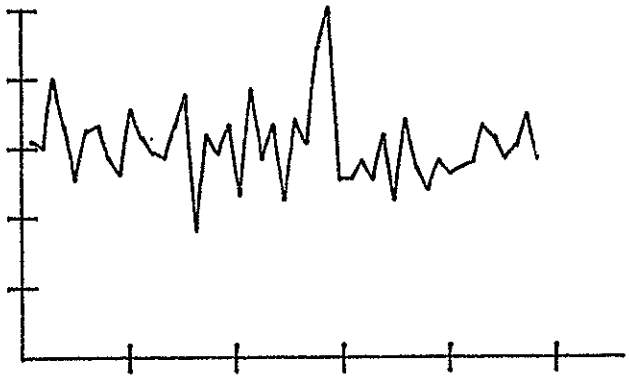

RUN 52 PEAK= 68 200 mv

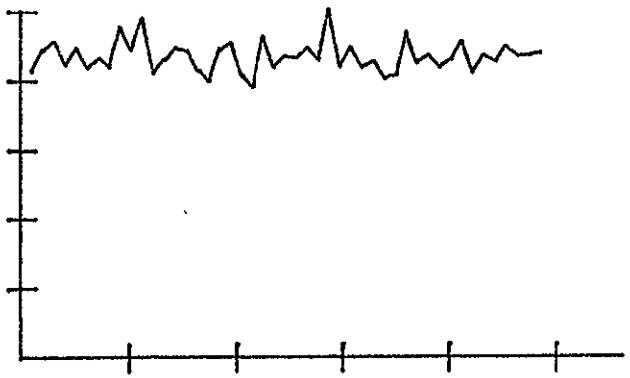

RUN 53 PEAK= 692 140 mv

Rerun on RN = 1.5×10^6, M = 0.9

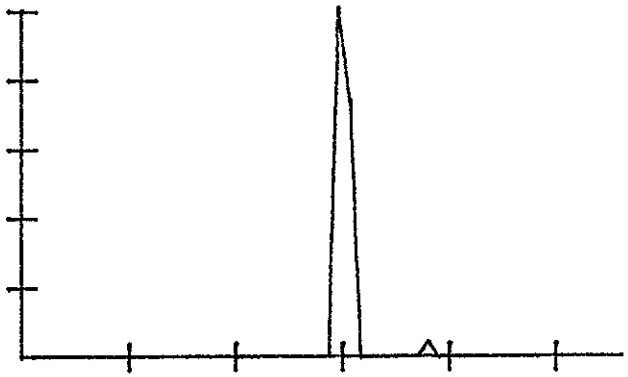

RUN 54 PEAK= 27 400 mv

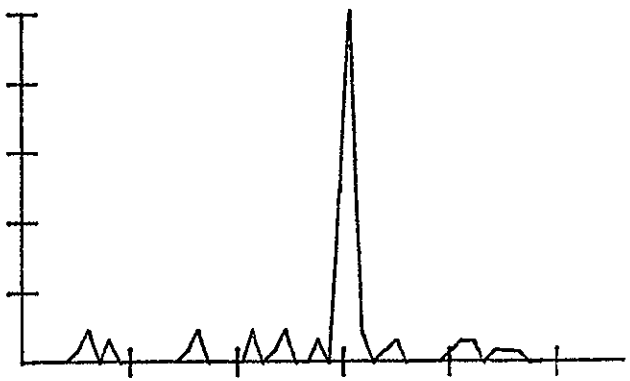

RUN 55 PEAK= 35 280 mv

Record/ RN → 3×10^6, M ≈ 0.9, not on condition yet

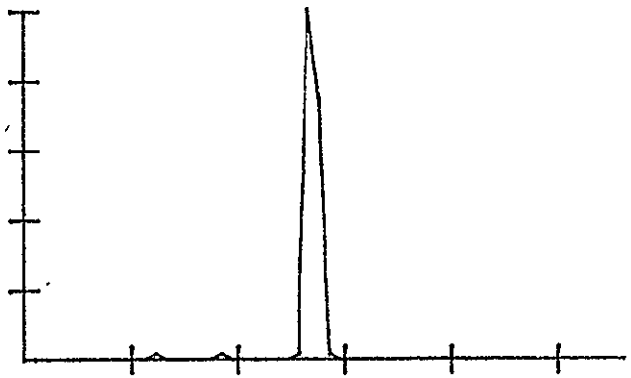

RUN 58 PEAK= 69 400 mv

NOTE: Runs 56 and 57 not saved

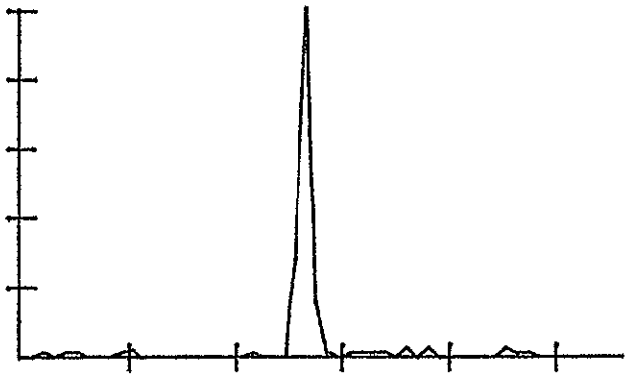

RUN 59 PEAK= 87 280 mv

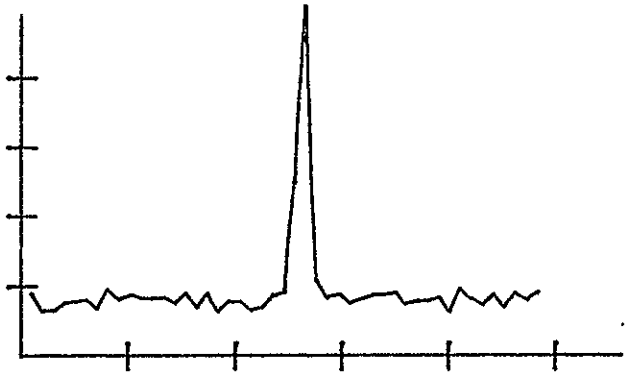

RUN 60 PEAK= 580 200 mv

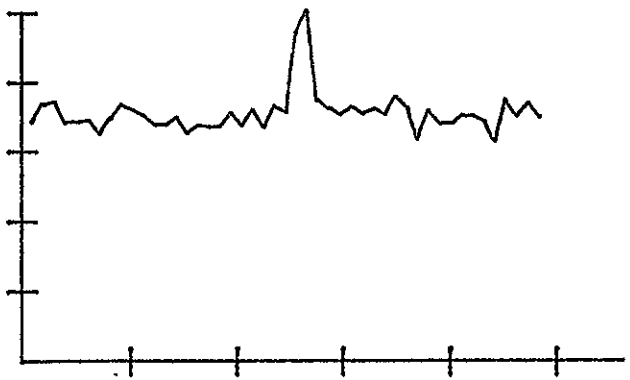

RUN 61 PEAK= 903 141 mv

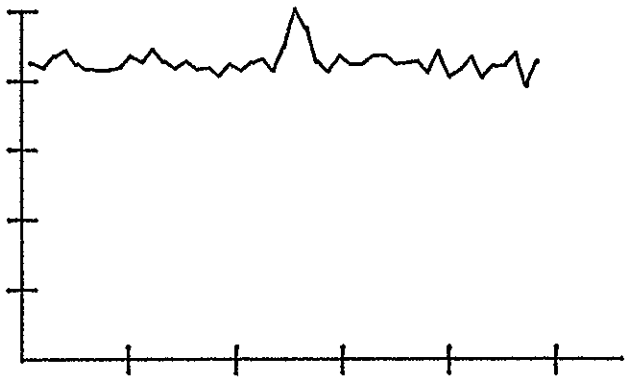

RUN 62 PEAK= 2500 100 mv

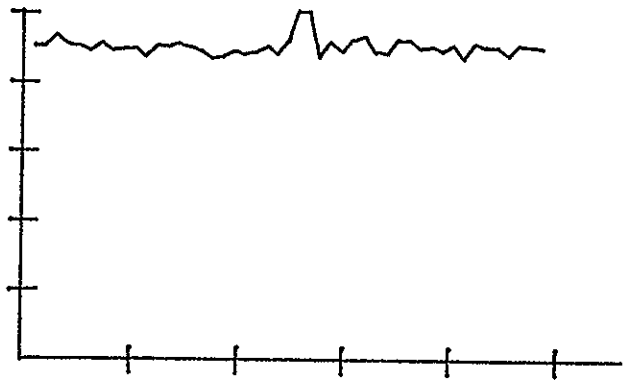

RUN 63 PEAK= 4389 70 mv

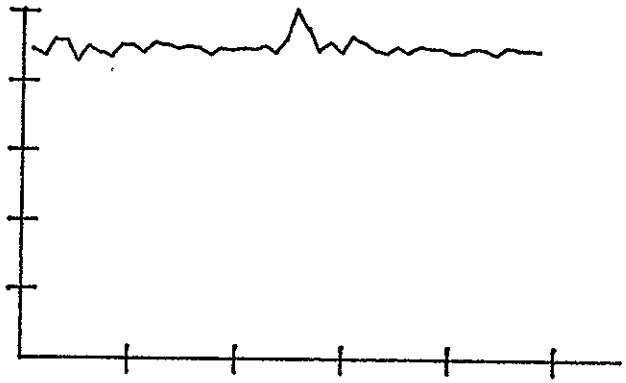

RUN 64 PEAK= 6021 50 mv

RN = 3×10^6, M = 0.9

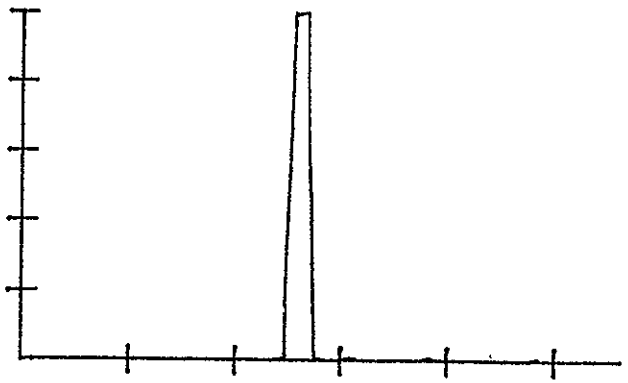

RUN 65 PEAK= 128 400 mv

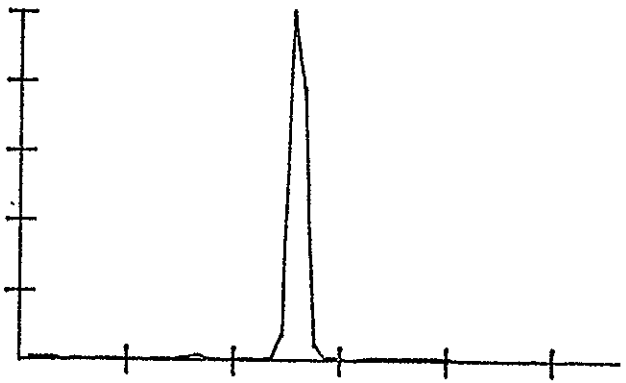

RUN 66 PEAK= 220 282 mv

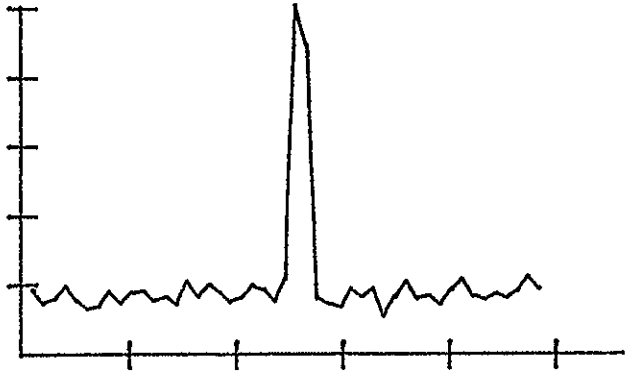

RUN 67 PEAK= 289 200 mv

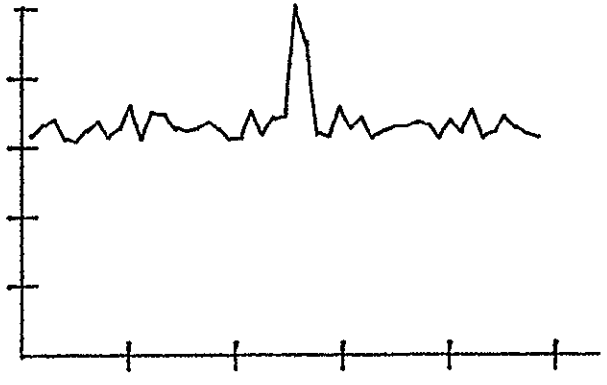

RUN 68 PEAK= 966 141 mv

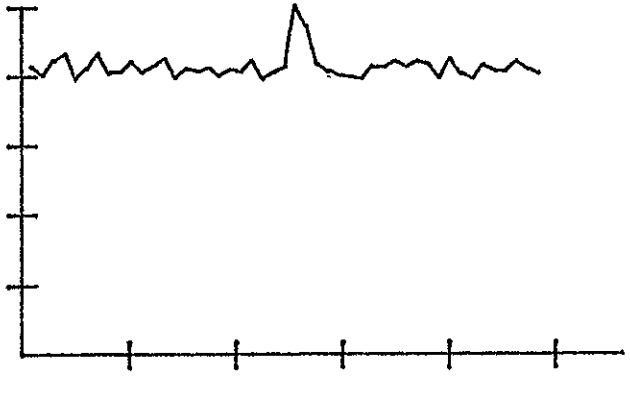

RUN 69 PEAK= 2598 100 mv

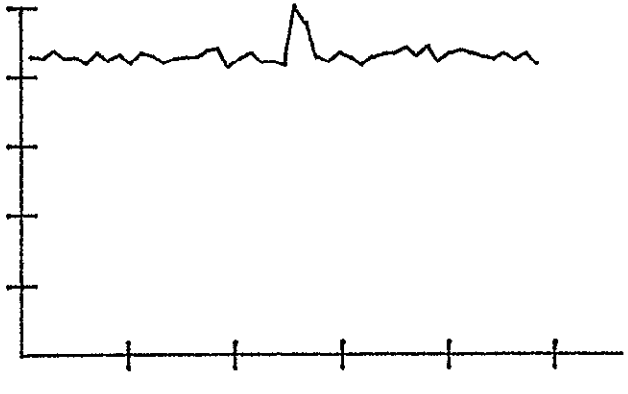

RUN 70 PEAK= 4560 70 mv

Repeat, exactly on condition at M = 0.9, RN = 3×10^6

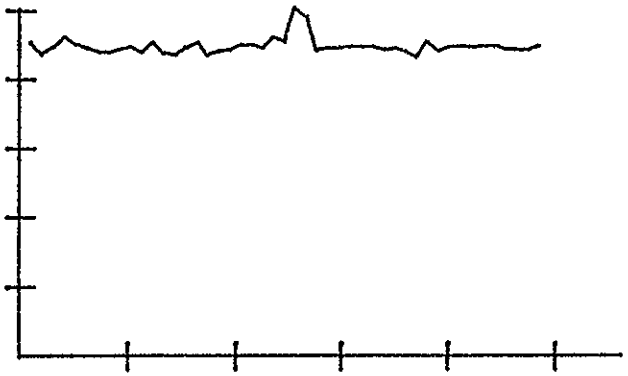

RUN 71 PEAK= 6107 50 mv

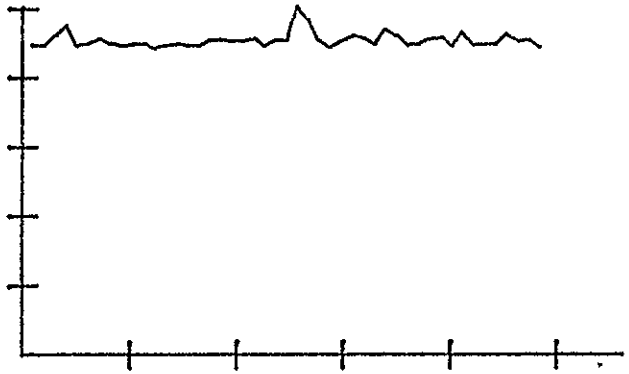

RUN 72 PEAK= 6079 50 mv

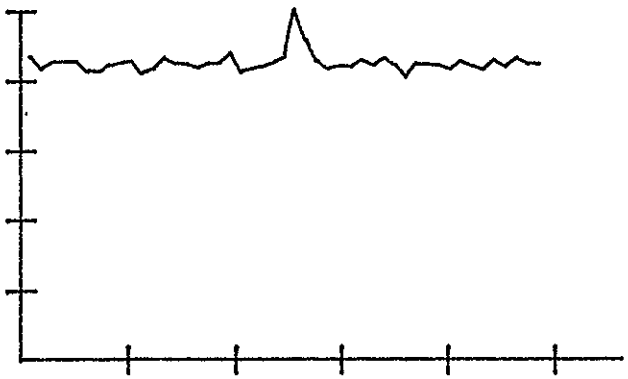

RUN 73 PEAK= 4562 70 mv

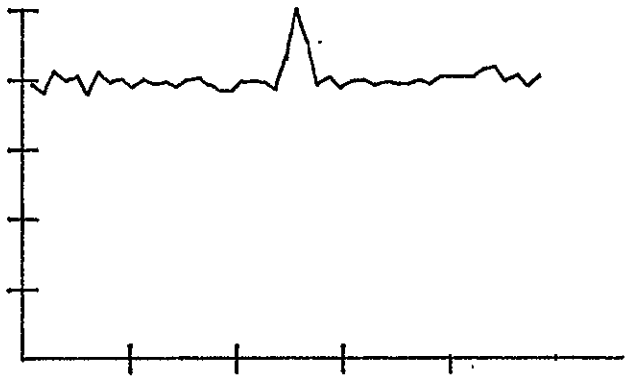

RUN 74 PEAK= 2669 100 mv

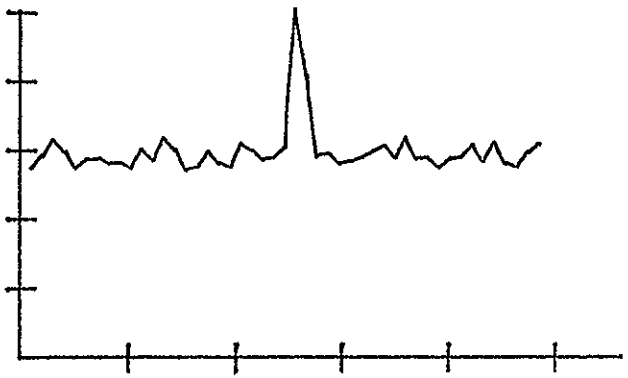

RUN 75 PEAK= 1076 140 mv

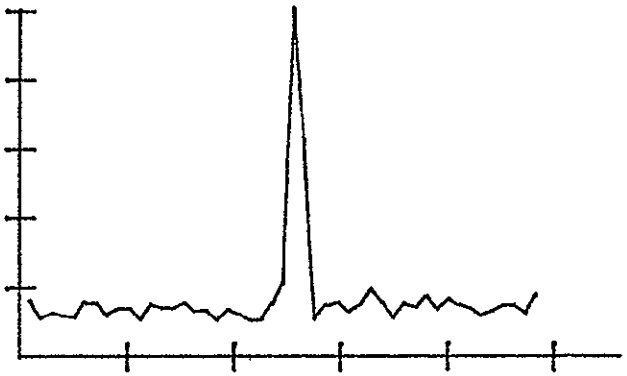

RUN 76 PEAK= 364 200 mv

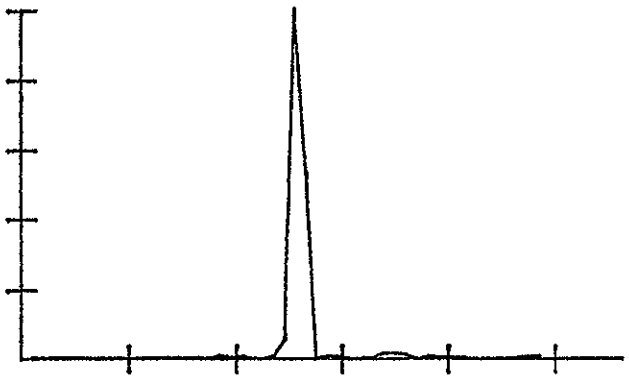

RUN 77 PEAK= 238 280 mv

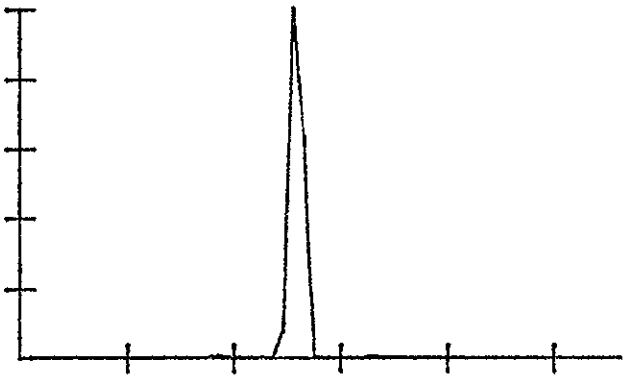

RUN 78 PEAK= 163 400 mv

RN = 3×10^8, M → 0.6

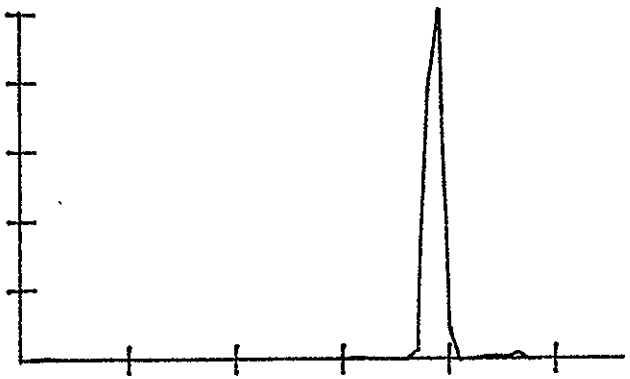

RUN 79 PEAK= 319 400 mv

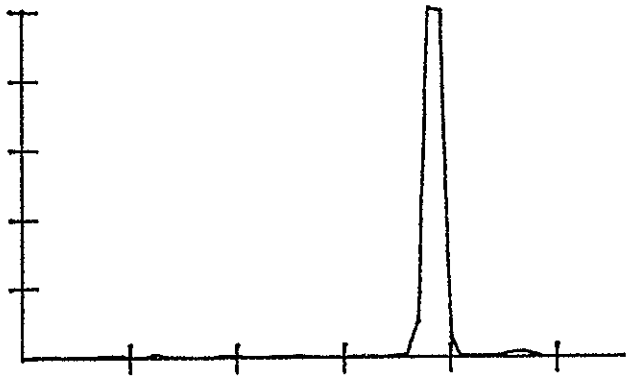

RUN 80 PEAK= 410 282 mv

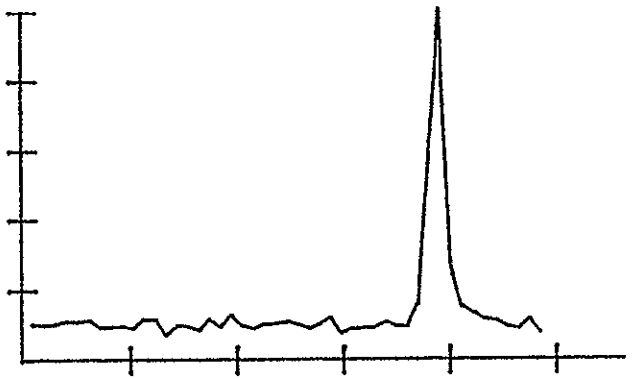

RUN 81 PEAK= 577 200 mv

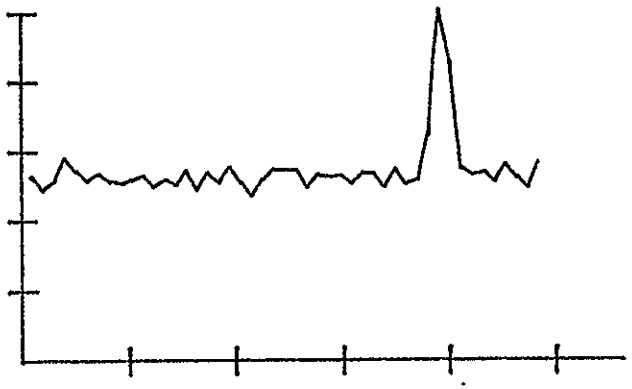

RUN 82 PEAK= 1289 141 mv

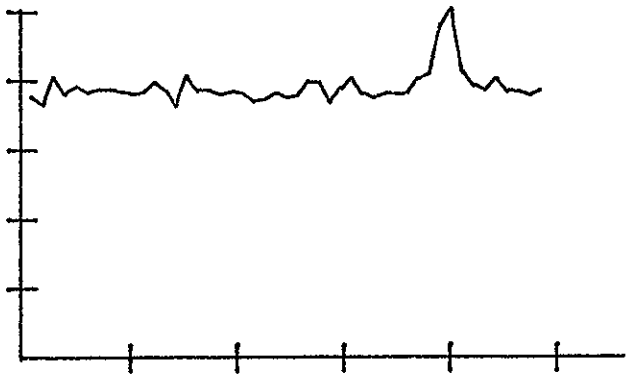

RUN 83 PEAK= 2926 100 mv

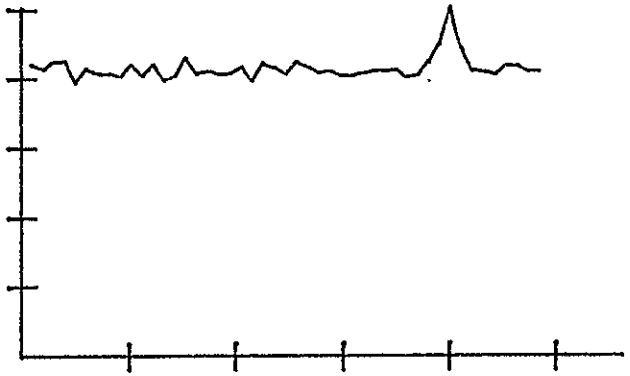

RUN 84 PEAK= 4910 70 mv

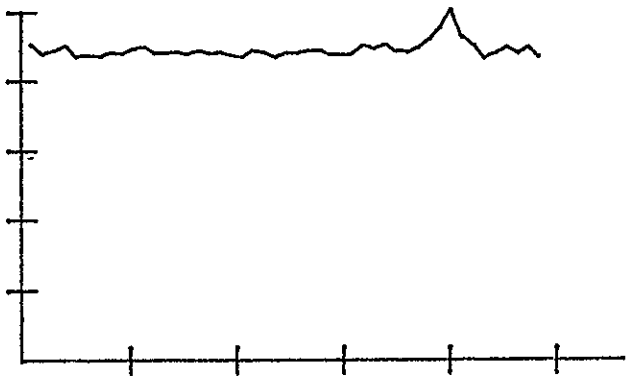

RUN 85 PEAK= 6321 50 mv

RN = 3×10^6, M = 0.6

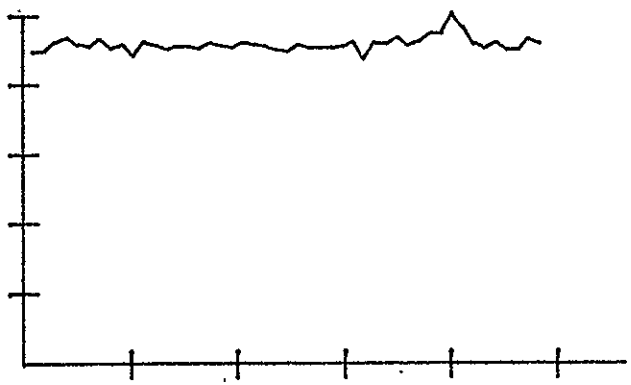

RUN 86 PEAK= 6885 50 mv

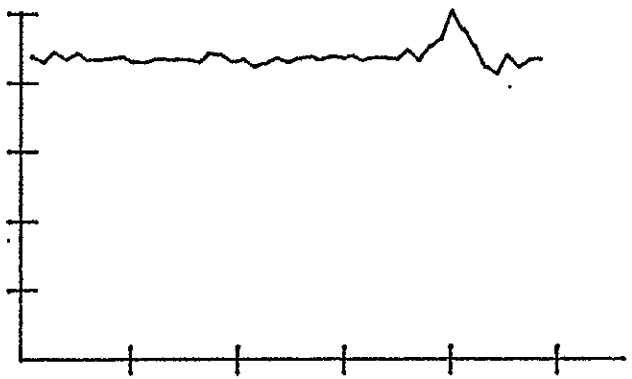

RUN 87 PEAK= 4584 70 mv

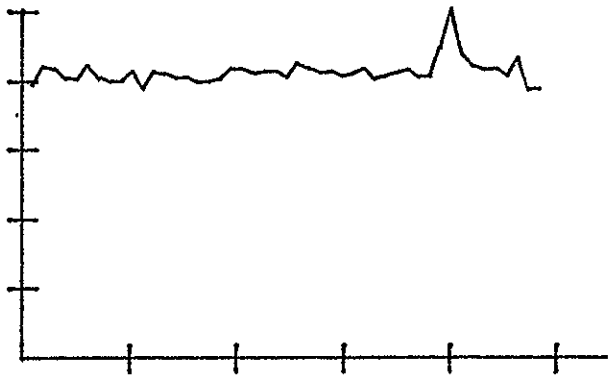

RUN 88 PEAK= 2740 100 mv

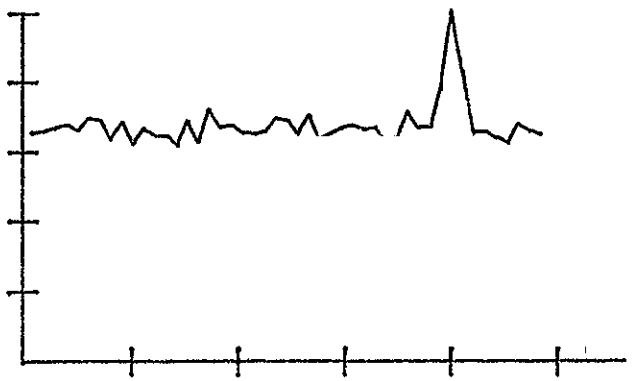

RUN 89 PEAK= 1013 140 mv

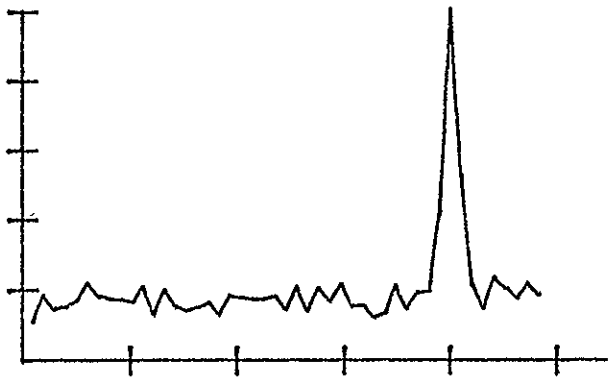

RUN 90 PEAK= 312 200 mv

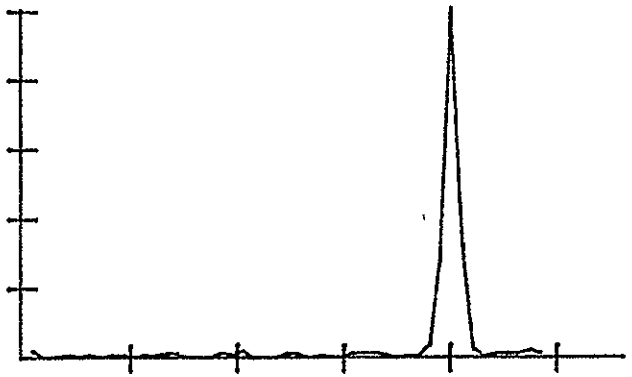

RUN 91 PEAK= 179 282 mv

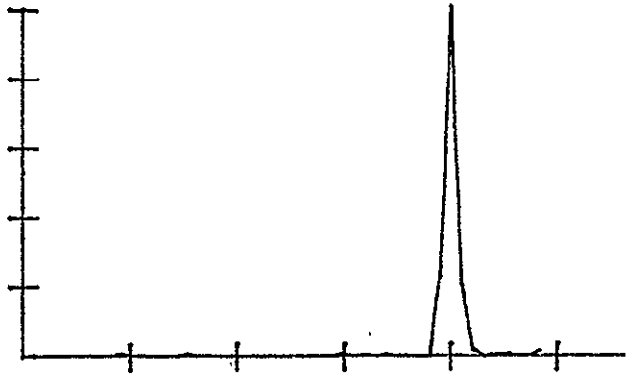

RUN 92 PEAK= 149 400 mv